



## Article

# Adsorptive removal of stable and radioactive Pb(II) isotopes from aqueous solution using bentonite, zeolite and perlite: characterization, isotherm and thermodynamic studies

Osman Uygun, Rufiyet Güven and Gaye Ö. Çakal 

Institute of Nuclear Sciences, Ankara University, Besevler, Ankara, Türkiye

### Abstract

In this study, stable and radioactive lead removal from aqueous solution by adsorption using bentonite, zeolite and perlite minerals obtained from various locations in Türkiye was studied in batch experiments. The adsorbents were first characterized using X-ray diffraction (XRD), X-ray fluorescence (XRF), Fourier-transform infrared (FTIR) spectroscopy, scanning electron microscopy (SEM) and energy-dispersive spectroscopy (EDS), and then the physicochemical properties were determined. The effects of various factors that influence adsorption, such as solution pH, adsorbent dosage, contact time, initial  $\text{Pb}^{2+}$  ion concentration, temperature and shaking rate, were studied. The adsorption of  $\text{Pb}^{2+}$  was modelled using the Langmuir, Freundlich and Dubinin–Radushkevich isotherms. The adsorption capacities of the minerals for  $\text{Pb}^{2+}$  followed the order: bentonite > zeolite > perlite, and the maximum adsorption capacities were 131.6, 36.1 and 21.5  $\text{mg g}^{-1}$ , respectively. The adsorption data fit well with the Langmuir isotherm. The bonding of lead ions on the adsorbents was confirmed by XRF and FTIR analyses after the adsorption process. The adsorption of  $\text{Pb}^{2+}$  ions on the adsorbents was spontaneous and endothermic. The adsorption process took place by cation exchange in addition to electrostatic interaction. Furthermore, radioactive  $^{210}\text{Pb}^{2+}$  adsorption on bentonite, zeolite and perlite was studied, with the analyte being analysed using a liquid scintillation counter. It was seen that in addition to Pb(II) ions, these minerals also adsorbed the radioactive decay products of  $^{210}\text{Pb}$ , which were  $^{210}\text{Po}$  and  $^{210}\text{Bi}$ . The removal percentages of  $^{210}\text{Pb}$  were 95%, 38% and 30% and those of  $^{210}\text{Po}$  were 75%, 60% and 74% for bentonite, zeolite and perlite, respectively.

**Keywords:**  $^{210}\text{Pb}$  isotope, bentonite, characterization, clay minerals, lead adsorption, LSC, perlite, zeolite

(Received 2 May 2023; revised 7 July 2023; Associate Editor: Chun-Hui Zhou)

Contamination of the environment by heavy metals is a major concern. Lead is an extremely toxic heavy metal that enters the environment through various industrial activities, agricultural applications and improper waste disposal (Jaishankar *et al.*, 2014; Joseph *et al.*, 2019). Metals from all sources accumulate in the environment and, in most cases, extreme levels of lead in ecosystems lead to environmental contamination (Raj & Das, 2023). Hence, the pollution of the environment by Pb, among the other heavy metals, has been studied worldwide. For instance, Pb pollution in Türkiye was reported at 23.8–178 ppm in İzmit Bay (Pekey, 2006), 141–797 ppm in Golden Horn Estuary (Ergin *et al.*, 1991), 11.6–305 ppm in Demirören Alteration area (Vural, 2015) and 7.78–19.7 ppm in the sediments and 8.48–24.1 ppm in the water of Süreyyabey Dam Lake (Erdoğan *et al.*, 2023). Pb pollution in sediments was reported at 36–83 ppm in Bangladesh (Islam *et al.*, 2015), 26.39–77.66 ppm in China (Liu *et al.*, 2009) and 55–450 ppm in Brazil (Pereira *et al.*, 2007).

Lead persists in the environment as it is non-biodegradable, and it accumulates in humans and animals *via* their consumption of contaminated food and water (Joseph *et al.*, 2019). Uptake of lead by humans causes cumulative toxicity in the body, which affects multiple systems and organs, causing serious health problems (Njoroge *et al.*, 2008).

Lead has both stable ( $^{204}\text{Pb}$ ,  $^{206}\text{Pb}$ ,  $^{207}\text{Pb}$  and  $^{208}\text{Pb}$ ) and radioactive ( $^{210}\text{Pb}$ ,  $^{211}\text{Pb}$ ,  $^{212}\text{Pb}$  and  $^{214}\text{Pb}$ ) isotopes present in the environment. In addition to its toxic property, lead also has a radiotoxic property due to its radioactive isotopes. Among these isotopes,  $^{210}\text{Pb}$ , formed during the  $^{238}\text{U}$  decay chain, is the most radiotoxic isotope of lead due to its long half-life of 22.23 (12) years (Nucleide Lara, 2023). As can be seen from the decay scheme in Fig. 1,  $^{210}\text{Pb}$  first decays to  $^{210}\text{Bi}$ , emitting  $\beta$ -particles (15.0 and 61.5 keV) and  $\gamma$ -rays (46.6 keV), then  $^{210}\text{Bi}$  decays to  $^{210}\text{Po}$ , emitting  $\beta$ -particles (1161 keV), and then  $^{210}\text{Po}$  decays to stable  $^{206}\text{Pb}$ , emitting  $\alpha$ -particles (5305 keV; Anokhina *et al.*, 2008). It can be understood from this scheme that until stable  $^{206}\text{Pb}$  is formed,  $^{210}\text{Pb}$ ,  $^{210}\text{Bi}$  and  $^{210}\text{Po}$  also contribute to the radioactivity and hence the radiotoxicity of lead in the environment. For this reason, the remediation of both stable and radioactive lead from the environment is of critical importance. It should be mentioned that the allowable lead concentration is

**Corresponding author:** Gaye Ö. Çakal; Email: [gcaikal@ankara.edu.tr](mailto:gcaikal@ankara.edu.tr)

**Cite this article:** Uygun O, Güven R, Çakal GayeÖ. (2023). Adsorptive removal of stable and radioactive Pb(II) isotopes from aqueous solution using bentonite, zeolite and perlite: characterization, isotherm and thermodynamic studies. *Clay Minerals* 58, 195–209. <https://doi.org/10.1180/clm.2023.18>

© The Author(s), 2023. Published by Cambridge University Press on behalf of The Mineralogical Society of the United Kingdom and Ireland. This is an Open Access article, distributed under the terms of the Creative Commons Attribution licence (<http://creativecommons.org/licenses/by/4.0/>), which permits unrestricted re-use, distribution and reproduction, provided the original article is properly cited.

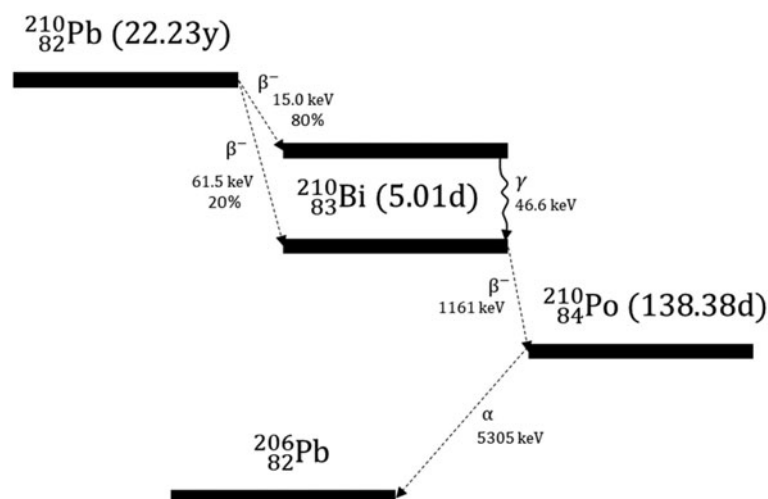


**Figure 1.** The decay scheme of  $^{210}\text{Pb}$  to  $^{210}\text{Bi}$  and  $^{210}\text{Po}$ . The half-lives of the radioisotopes are given in parentheses (Anokhina *et al.* 2008; Nuclide Lara 2023).

limited to  $10\ \mu\text{g L}^{-1}$  in drinking water according to the World Health Organization (WHO) and European Union (EU; WHO, 2017; EU, 2020; Dettori *et al.*, 2022). Moreover, WHO limits  $^{210}\text{Pb}$  isotopes in drinking water as  $0.1\ \text{Bq L}^{-1}$  (WHO, 2017).

Conventionally, Pb(II)-contaminated water is treated using various physicochemical treatment techniques, including chemical precipitation, coagulation, flocculation, ion exchange, adsorption and filtration (Fu & Wang, 2011; Kumar *et al.*, 2022). Among these techniques, chemical-based treatment techniques are used most often; however, their adverse effects on the environment increase demand for cleaner treatment processes such as membrane filtration, adsorption and electrochemical, hydrogel, photocatalysis, biological and bio-integrated treatment techniques (Kumar *et al.*, 2022). Adsorption has been the most used technology for the removal of heavy metals from wastewater (Fei & Hu, 2023). In this method, the adsorbate (contaminant) adheres to the surface of the adsorbent through physical (electrostatic attraction) or chemical (ion exchange, complexation, precipitation) means. However, environmental conditions (e.g. pH, temperature, adsorbent-to-adsorbate ratio, stirring rate, etc.) affect the adsorption capacities of the adsorbents.

Treatment of industrial wastewater by adsorption for the removal of heavy metals using long-term durable, cheap, sustainable and environmentally friendly adsorbents with high adsorption capacity and selectivity, rapid kinetics of adsorption and desorption and low energy penalties for regeneration is of great importance (Velarde *et al.*, 2023). This requires adsorbents to have a large accessible surface area providing abundant exposed active sites for strong and selective binding with heavy metal ions. The effective surface area of an adsorbent exposed to heavy metal ions in an aqueous solution is also influenced by water dispersibility, hydrophilicity, functionality and other properties (Fei & Hu, 2023). There are various kinds of adsorbents, such as activated carbon, carbon nanotubes, graphene oxide, mesoporous silica, mesoporous carbon, clays, zeolites, metal-organic frameworks and adsorbents from industrial/agricultural byproduct residues (Fei & Hu, 2023; Velarde *et al.*, 2023). Naturally occurring minerals are preferred as adsorbents due to their chemical structures, adsorption properties and global abundance. In addition to the use of these raw minerals, minerals modified and treated through heat treatment, acid activation, ion exchange and mechanochemical processing have also been studied extensively in the literature for the adsorption of heavy

metals in terms of their ability to increase the adsorption, cation-exchange capacity (CEC) and specific surface area of such minerals (Bhattacharyya & Gupta, 2008; Novikau & Lujaniene, 2022). Surfaces modified with metal-binding groups have a greater ability to capture heavy metal ions. For instance, it has been shown that phosphate-modified kaolinite clay (Unuabonah *et al.*, 2007), lanthanum oxide-modified bentonite (Lingamdinne *et al.*, 2023), hexadecyltrimethylammonium (HDTMA)- and phenyl fatty hydroxamic acid (PFHA)-modified bentonite (Hamadneh *et al.*, 2015) and alkaline-treated zeolite (El-Arish *et al.*, 2022) demonstrate greater adsorption capacities, leading to greater  $\text{Pb}^{2+}$  ion removal percentages. Synthesized adsorbents based on mesoporous silica, such as SBA-15, MCM-41 and MCM-48, with or without modification, have also been used for the removal of heavy metals due to their large surface areas and porous structures (Benhamou *et al.*, 2009; Hernández-Morales *et al.*, 2012; Anbia *et al.*, 2015; Guo *et al.*, 2017; Albayati *et al.*, 2019).

Bentonites are naturally occurring clays that consist primarily of smectite minerals, usually montmorillonite. Bentonites are abundantly occurring clay minerals of the 2:1 layer type (i.e. a central octahedral alumina sheet sandwiched between two tetrahedral silica sheets; Abdullahi & Audu, 2017; Klopogge, 2017). Zeolites are hydrated aluminosilicates composed of networks of  $[\text{SiO}_4]^{4-}$  and  $[\text{AlO}_4]^{5-}$  tetrahedra linked to each other with oxygen atoms (Delkash *et al.*, 2015; Khaleque *et al.*, 2020). Each oxygen atom within Si-O and Al-O bonds connects two cations and is shared between the two tetrahedra (Moshoeshe *et al.*, 2017). The isomorphous substitution within the sheets of bentonite, involving the substitution of  $\text{Al}^{3+}$  for  $\text{Si}^{4+}$  in the tetrahedral layer and  $\text{Mg}^{2+}$  or  $\text{Fe}^{3+}$  for  $\text{Al}^{3+}$  in the octahedral layer (Eren *et al.*, 2009) or the isomorphous substitution of  $\text{Al}^{3+}$  for  $\text{Si}^{4+}$  within the tectosilicate framework of zeolite (Moshoeshe *et al.*, 2017), generates a negative charge. This negative charge is balanced by the exchangeable cations such as  $\text{Ca}^{2+}$ ,  $\text{Mg}^{2+}$  and  $\text{Na}^+$  located in the interlayer spaces (Delkash *et al.*, 2015; Abdullahi & Audu, 2017; Klopogge, 2017; Khaleque *et al.*, 2020).

Perlite is an aluminosilicate hydrated volcanic glass of obsidian that has a rhyolitic composition with generally >70% silica. It also contains exchangeable cations such as  $\text{K}^+$  and  $\text{Na}^+$  and up to 5% water. The adsorbent nature of perlite is due to the hydroxyl groups bound to the silicon atoms on the surface of the perlite. The silicon atoms at the surface tend to maintain their tetrahedral coordination with oxygen and attach to the monovalent hydroxyl

groups, forming silanol groups (Alkan & Doğan, 2001; Ghassabzadeh *et al.*, 2010). A hyper-light material (i.e. expanded perlite) can be obtained by heating the perlite to 760–1100°C, causing the material to expand up to 20 times its original volume (Çelik *et al.*, 2013; Aghabeyk *et al.*, 2022).

Lead removal from aqueous solutions has been reported in the literature by utilizing either natural or treated clinoptilolite (Günay *et al.*, 2007; Wang *et al.*, 2008; Rakhym *et al.*, 2020), bentonite (Donat *et al.*, 2005; Guerra *et al.*, 2013; Pawar *et al.*, 2016) or perlite (Sari *et al.*, 2007; Ghassabzadeh *et al.*, 2010; Irani *et al.*, 2011). Although there have been various studies on the adsorption of lead on raw, modified or treated minerals, we found no study in the literature to have investigated the adsorption of radioactive lead on aluminosilicate-based adsorbent materials and the use of a liquid scintillation counter (LSC;  $\beta$ -spectrometer) as a  $^{210}\text{Pb}$  determination technique in an adsorption study. In addition, we found no study to have compared the lead adsorption capacities of bentonite, zeolite and perlite.

Therefore, this study aims: (1) to characterize bentonite, zeolite and perlite minerals from various provinces in Türkiye in detail; (2) to study and compare the adsorption of  $\text{Pb}^{2+}$  ions using these minerals by varying the experimental conditions; (3) to fit the experimental data using various adsorption isotherm models; (4) to discuss the adsorption mechanisms of  $\text{Pb}^{2+}$  ions on the adsorbents; (5) to characterize the adsorbents after  $\text{Pb}^{2+}$  ion adsorption; (6) to repeat the adsorption experiments by contaminating the  $\text{Pb}^{2+}$  ion solution with radioactive  $^{210}\text{Pb}$  isotopes; and (7) to compare the removal percentages according to the obtained stable  $\text{Pb}^{2+}$  ion (inductively coupled plasma optical emission spectroscopy; ICP-OES) and radioactive  $^{210}\text{Pb}^{2+}$  isotope (LSC) results.

## Materials and methods

### Materials

Bentonite (Ordu, Türkiye), zeolite (clinoptilolite, Nevşehir, Türkiye) and expanded perlite (İzmir, Türkiye) were used as adsorbents throughout the study. The zeolite and bentonite minerals were first washed with Milli-Q water before characterization and batch adsorption experiments to remove water-soluble impurities and then dried at 110°C (Mipro MLF-120, Türkiye) for 4 h, whereas expanded perlite was used as received. Pb ( $\text{NO}_3)_2$  ( $\geq 99.0\%$  purity, Sigma-Aldrich) and a sample with known  $^{210}\text{Pb}$  activity concentration were used as lead sources. All of the other chemicals used in this study were purchased as analytical grade.

### Mineralogical and petrographic analyses of the adsorbents

The crystal structure of the adsorbents was investigated using an Inel Equinox 1000 X-ray diffractometer (XRD) equipped with a Co X-ray tube. XRD traces were recorded at 5–60°2 $\theta$  at steps of 0.02°. The chemical analysis of the adsorbents was performed using a Spectro X-LAB 2000 polarized energy dispersive X-ray fluorescence (PED-XRF) spectrometer. Infrared spectra of the adsorbents were recorded in the 4000–400  $\text{cm}^{-1}$  region on a Varian/660-IR Fourier-transform infrared (FTIR) spectrometer. The surface morphology and elemental composition of the adsorbents were obtained using scanning electron microscopy (SEM)-energy-dispersive spectrometry (EDS) analysis with a ZEISS EVO

40 device. XRF and FTIR analyses of the adsorbents were also carried out after the batch adsorption experiments.

## Physicochemical properties of the adsorbents

### Water absorption capacities

The water adsorption capacities of the adsorbents were determined according to the ASTM C127-88 (1993) standard. First, a known amount of dried sample was kept in Milli-Q water for 24 h at room temperature. After removing the excess water from the samples,  $\sim 1$  g of wet sample was weighed and dried in an oven at 110°C for 4 h. The mass loss was calculated to determine the water absorption capacity of the adsorbent samples. This procedure was repeated three times and the values were averaged.

### Cation-exchange capacities

The CEC values of the adsorbents were found by means of the ASTM C837-09 standard and following work by Topal (1996) using the methylene blue (MB) adsorption test. This test was carried out to determine the amount of MB dye absorbed by the sample through ion exchange, which was also correlated with the CEC of the adsorbent samples. For this test, 2 g of clay sample were added to 300 mL Milli-Q water. After uniform dispersion of the adsorbent samples in water (stirring for 5 min), small increments (2–5 mL) of MB dye were added to the samples. Then a small drop was dripped from this solution onto filter paper every few minutes until a blue halo appeared around the drop. The blue halo indicated that the endpoint had been reached, which also denoted that there was excess MB dye in the solution that was not absorbed by the mineral. Once the halo was seen, the volume of MB dye added to the solution was recorded to calculate the CEC of the mineral. The CEC ( $\text{meq } 100 \text{ g}^{-1}$ ) was determined using Equation 1 (Topal, 1996):

$$\text{CEC} = \left( \frac{100}{W_B} \right) \cdot V_{\text{MB}} \cdot N_{\text{MB}} \quad (1)$$

where  $W_B$  is the dry mass of the adsorbent sample used (g),  $V_{\text{MB}}$  is the volume of MB dye added into the clay mixture until the endpoint is reached (mL) and  $N_{\text{MB}}$  is the normality of the MB solution (N), which was 0.03125 N in this test.

### Dissolution in water

The dissolution of the adsorbents in Milli-Q water was observed at room temperature after keeping the samples in water for 24 h. The dissolved ions were determined according to ICP-OES analysis of the filtrates. The solid residues were also dried in an oven at 80°C for 4 h and the mass loss of the samples was determined to evaluate the amount dissolved.

### Particle size

The Sauter mean particle size of the adsorbents was determined using a Malvern Mastersizer 3000E. The samples were dispersed in water and the measurements were performed at a stirring speed of 500 rpm.

### BET surface area

The Brunauer–Emmett–Teller (BET) surface areas of the adsorbents were determined using Quantachrome Autosorb 6B.

### Point of zero charge

The salt addition technique was used to determine the point of zero charge (PZC) of the adsorbent materials (Bakatula *et al.*, 2018). In this technique, 0.2 g of adsorbent material was added to 40.0 mL of 0.1 M NaNO<sub>3</sub> solution in a series of 50 mL glass bottles. The pH was adjusted with 0.1 M HNO<sub>3</sub> and 0.1 M NaOH to obtain the appropriate pH range of 3, 5, 7, 9 and 11 ( $\pm 0.1$  pH units). First, the initial pH values (pH<sub>i</sub>) of the supernatant solutions were recorded. Then, the samples were shaken at 200 rpm for 24 h using an orbital shaking incubator (Mipro MLI-120, Türkiye). The final pH values (pH<sub>f</sub>) were measured and the difference in the pH values ( $\Delta\text{pH} = \text{pH}_f - \text{pH}_i$ ) was calculated. The PZC values were found from the linear  $\Delta\text{pH}-\text{pH}_i$  plots for each adsorbent. The PZC values were determined at  $\Delta\text{pH} = 0$ , as at this PZC value the positive and negative charges on the surface of the adsorbent were equal.

### Z-potential

The  $\zeta$ -potential values of the samples were determined at pH 7 using a Malvern Zetasizer Nano ZS90 device.

### Batch adsorption experiments using stable Pb<sup>2+</sup> ion solution

The batch adsorption experiments of lead-contaminated waters were performed in 50 mL glass bottles according to ASTM 4646-03 (2016) to determine the effects of the initial pH value of the solution (3–9), adsorbent dosage (1–10 g L<sup>-1</sup>), initial Pb<sup>2+</sup> concentration (100–800 ppm), temperature (25–60°C), contact time (15–1440 min) and shaking rate (0–150 rpm). The effect of pH was examined by dispersing 0.25 g of adsorbent in a 50 mL Pb<sup>2+</sup> solution at a concentration of 200 ppm and adjusting the pH of the solution using 1 M HCl or 1 M NaOH. The effect of the shaking rate was determined using an orbital shaking incubator (Mipro MLI-120, Türkiye). After the batch adsorption experiments, the filtrate was separated from the adsorbent using filter paper, and Pb<sup>2+</sup> concentration in the filtrate was determined used ICP-OES. A schematic diagram showing the batch adsorption experiments is given in Fig. 2. Reproducibility experiments were also performed.

The differences in Pb<sup>2+</sup> ion concentrations under the same experimental conditions were found to be  $\sim 5\%$ .

The adsorption capacity ( $q_t$ , mg g<sup>-1</sup>), removal rate ( $R$ , %) and distribution coefficient ( $K_d$ , mL g<sup>-1</sup>) were calculated using Equations 2, 3 and 4, respectively.

$$q_t = (C_0 - C_t) \frac{V}{M} \quad (2)$$

$$R = \frac{C_0 - C_t}{C_0} \cdot 100 \quad (3)$$

$$K_d = \frac{(C_0 - C_t) \cdot V}{C_t \cdot M} \quad (4)$$

where  $C_0$  is the initial mass concentration of the adsorbate (ppm),  $C_t$  is the mass concentration of the adsorbate at any  $t$  (ppm),  $V$  is the volume of the aqueous solution (L),  $M$  is the mass of the adsorbent (g) and  $q_t = q_e$  at  $C_t = C_e$ , with  $q_e$  and  $C_e$  denoting the equilibrium adsorption capacity and equilibrium mass concentration, respectively.

Adsorption isotherms were determined using the Langmuir, Freundlich and Dubinin–Radushkevich equations. The thermodynamic parameters such as the change in Gibbs free energy ( $\Delta G^\circ$ ), enthalpy ( $\Delta H^\circ$ ) and entropy ( $\Delta S^\circ$ ) related to the adsorption of Pb<sup>2+</sup> ions on the adsorbents were evaluated using Equations 5 and 6 and plotting  $\ln(K_d)$  vs  $1/T$  graphs.

$$\ln(K_d) = \frac{\Delta S^\circ}{R} - \frac{\Delta H^\circ}{RT} \quad (5)$$

$$\Delta G^\circ = \Delta H - T\Delta S = -RT\ln(K_d) \quad (6)$$

In Equations 5 and 6,  $T$  is temperature in Kelvin and  $R$  is the universal gas constant (8.314 J mol<sup>-1</sup> K<sup>-1</sup>).

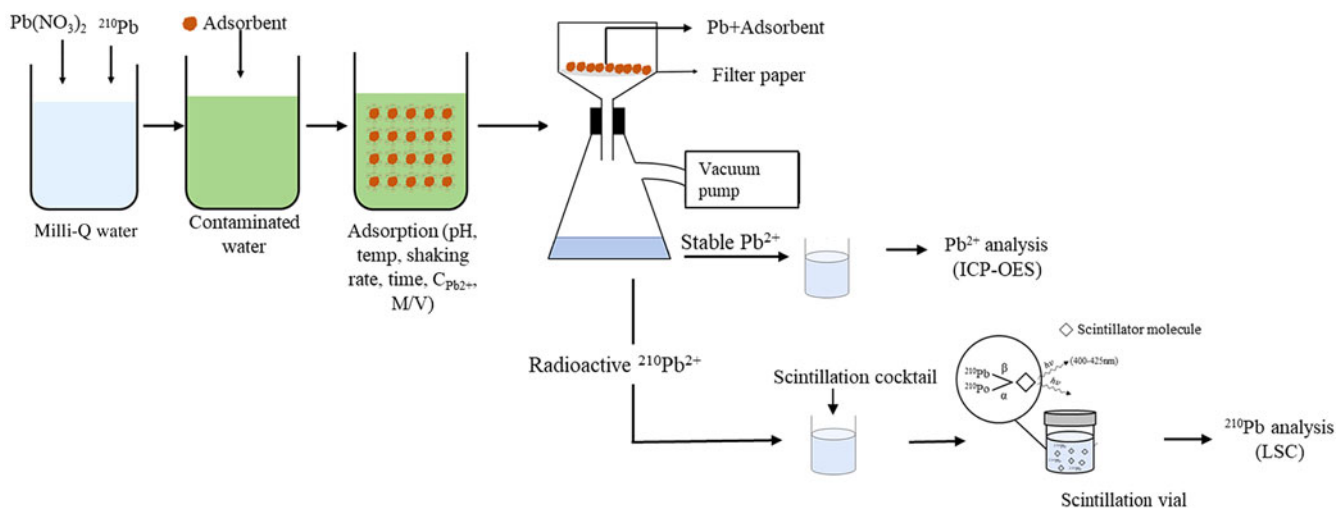


**Figure 2.** Schematic diagram of the batch adsorption experiments for stable Pb<sup>2+</sup> and radioactive <sup>210</sup>Pb. The batch adsorption experiments for the adsorption of stable Pb<sup>2+</sup> were performed using Pb(NO<sub>3</sub>)<sub>2</sub> and the batch adsorption experiments for the adsorption of radioactive <sup>210</sup>Pb were performed using both Pb(NO<sub>3</sub>)<sub>2</sub> and <sup>210</sup>Pb as contaminants.



### Batch adsorption experiments using radioactive $^{210}\text{Pb}$ isotope solution

The batch adsorption experiments were also performed with  $^{210}\text{Pb}$ -contaminated ( $17.86 \pm 1.28 \text{ Bq L}^{-1}$ ) 400 ppm  $\text{Pb}^{2+}$  ion solution at pH 7, contact time 2 h, adsorbent dosage  $5 \text{ g L}^{-1}$ , shaking rate 75 rpm and temperature  $25^\circ\text{C}$  (Fig. 2). In addition to these experiments, two successive adsorption experiments were carried out at the same adsorption conditions with the filtrates of the previous adsorption in order to determine the complete adsorption of the isotopes by the adsorbents.

After each experiment, 5 mL of the filtrate were mixed with 15 mL of scintillation cocktail (Optiphase HiSafe 3, Perkin Elmer) and assessed at least three times for 200 min in a LSC (Quantulus 1220, Perkin Elmer). The count values were then averaged. The calibration of LSC was performed according to Çakal *et al.* (2015) before the analyses. The counts for gross  $\alpha$  ( $^{210}\text{Po}$ ) and gross  $\beta$  ( $^{210}\text{Pb}$  and  $^{210}\text{Bi}$ ) were acquired separately, and then the total  $\beta$ -spectrum was evaluated as stated by Limon (2016). The net  $^{210}\text{Pb}$  count was calculated by subtracting the counts belonging to  $^{210}\text{Bi}$  (counts between 350 and 650 channels) from the total count in the  $\beta$ -spectrum. The activity concentrations were calculated using Equation 7:

$$A = \frac{N/t_c}{V \cdot \epsilon} \quad (7)$$

where  $A$  is the activity concentration ( $\text{Bq L}^{-1}$ ),  $N$  is the net count,  $t_c$  is the counting time (s),  $\epsilon$  is the detector efficiency (%) and  $V$  is the sample volume (L). The minimum detectable concentrations (MDCs) of the LSC system were calculated as  $\text{MDC}_\alpha = 0.03 \text{ Bq L}^{-1}$  and  $\text{MDC}_\beta = 0.26 \text{ Bq L}^{-1}$ .

## Results and discussion

### Mineralogical and petrographic analyses of the adsorbent materials

#### XRD analysis

XRD traces were acquired for bentonite, zeolite and perlite (Fig. 3). It was found that bentonite was mainly composed of montmorillonite (Mt), with the other reflections on the diffraction traces belonging to vermiculite (V), kaolin (K) and illite (I). The main constituent of zeolite was clinoptilolite (Cl). Trace amounts of mordenite (Mr) and quartz (Q) were also present in its structure. Perlite consisted of amorphous mineral phases with albite (A) and opal-CT (O) present as impurities.

#### XRF analysis

The chemical analysis of the adsorbent materials is given in Table 1. It was observed that the main components of the adsorbents were Si (30.65–33.04%) and Al (6.90–7.52%). The main cations were Mg (1.06%) and Ca (2.56%) in bentonite, K (1.56%) and Ca (2.24%) in zeolite and Na (2.63%), Mg (1.60%) and K (3.60%) in perlite.

As is known, the Si/Al ratio plays an important role in the adsorption performance of materials. A greater Si/Al ratio results in greater thermal and physical stability, whereas a lower Si/Al ratio exhibit greater CEC (Delkash *et al.*, 2015; Costafreda & Martin, 2021) because the greater the amount of aluminium in the adsorbent structure, the more cationic sites that will be formed. A Si/Al ratio of 4–5, indicating very high physicochemical durability and relatively high cation exchange, was reported previously (Delkash *et al.*, 2015). The Si/Al ratios of bentonite, zeolite and perlite were found to be 4.12, 4.22 and 4.79, respectively.

#### SEM-EDS analysis

SEM images of the adsorbent samples are given in Fig. 4a–c. Bentonite (Fig. 4a) had structural defects on the surface of the

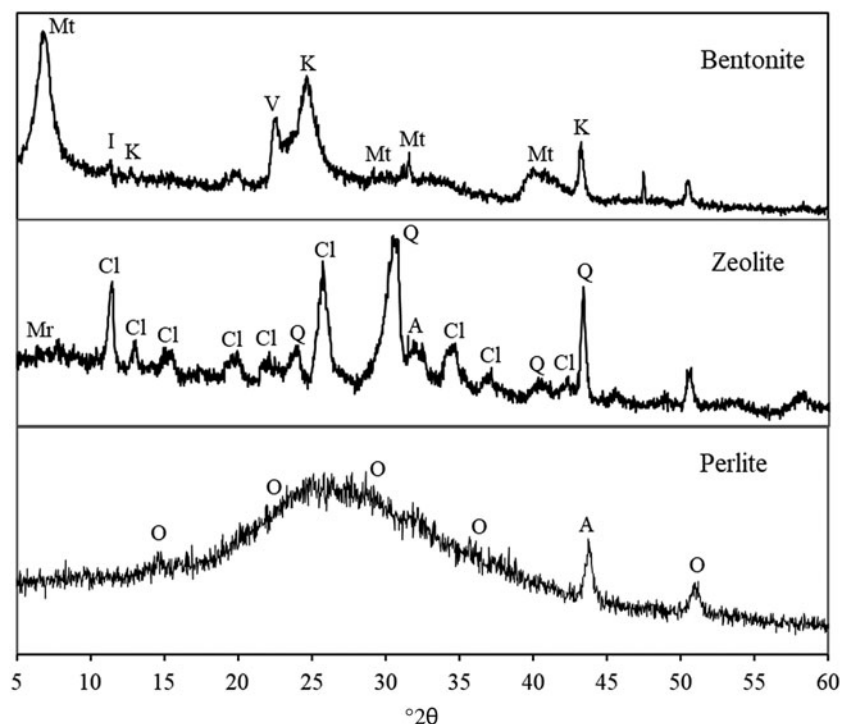


Figure 3. XRD traces of the adsorbents.

**Table 1.** Elemental compositions (%) of the adsorbent materials before and after batch adsorption experiments as obtained from XRF spectrometry.

Adsorbent		Na	Mg	Al	Si	K	Ca	Fe	Pb	LOI
Bentonite	Before adsorption	0.05	1.06	7.44	30.65	0.98	2.56	1.64	–	11.8
	After adsorption	0.05	0.52	2.68	18.59	0.60	0.51	0.82	5.38	
Zeolite	Before adsorption	0.33	0.49	7.52	31.76	1.56	2.24	0.66	–	9.83
	After adsorption	0.05	0.14	2.40	15.48	0.99	1.38	0.55	2.29	
Perlite	Before adsorption	2.63	1.60	6.90	33.04	3.60	0.80	0.73	–	3.08
	After adsorption	1.75	0.02	4.40	30.32	4.24	0.64	0.70	0.54	

LOI = loss on ignition.

particles, which increased its surface area. Zeolite (Fig. 4b) was formed from platelets that conglomerated into non-porous, large-sized particles of submicron size on their flat surface. Perlite (Fig. 4c) was formed from thin, transparent, glassy layers.

Results of the EDS analyses of the adsorbents are given in Fig. 4d–f and the elemental compositions of the samples are presented in Table 2. The elemental compositions of the adsorbents obtained using EDS were different from those determined using XRF spectrometry for some of the elements, despite the same bulk sample being analysed. These differences were due to the fact that XRF analysis was performed by using the bulk composition, whereas EDS analysis was conducted using a spot-sized sample.

#### FTIR analysis

The FTIR spectra of bentonite, zeolite and perlite were recorded in the 4000–400  $\text{cm}^{-1}$  region (Fig. 5). All the FTIR spectra of these adsorbents demonstrated similar bands in their structures. The bands at 3630–3560  $\text{cm}^{-1}$  were assigned to structural OH stretching vibrations in the Si–OH and Al–OH groups (Wang *et al.*, 2009;

Abdullahi & Audu, 2017), with the 3630  $\text{cm}^{-1}$  band originating from the Al<sub>2</sub>OH stretching vibration (Tabak *et al.*, 2011). The peaks at 1650–1610  $\text{cm}^{-1}$  corresponded to bending vibrations of the hydroxyl groups of physisorbed free water (Wang *et al.*, 2009; Tabak *et al.*, 2011; Hannachi *et al.*, 2013; Abdullahi & Audu, 2017; Vicentin & Costa da Rocha, 2021). The bands at 1010  $\text{cm}^{-1}$  represented the stretching vibrations of Si–O bonds (Korkuna *et al.*, 2006; Abdallah & Yilmazer, 2011; Hannachi *et al.*, 2013; Abdullahi & Audu, 2017). The bands at 790–750  $\text{cm}^{-1}$  corresponded to Si–O bond stretching of the silicate (Abdallah & Yilmazer, 2011; Vicentin & Costa da Rocha, 2021). The bands at 520  $\text{cm}^{-1}$  were due to Al–Si–O bending vibrations (Wang *et al.*, 2009; Abdallah & Yilmazer, 2011; Hannachi *et al.*, 2013).

#### Physicochemical properties of the adsorbents

The results obtained during the physicochemical investigation of the bentonite, zeolite and perlite samples are given in Table 3. The minerals used in this study had bulk densities and mean particle

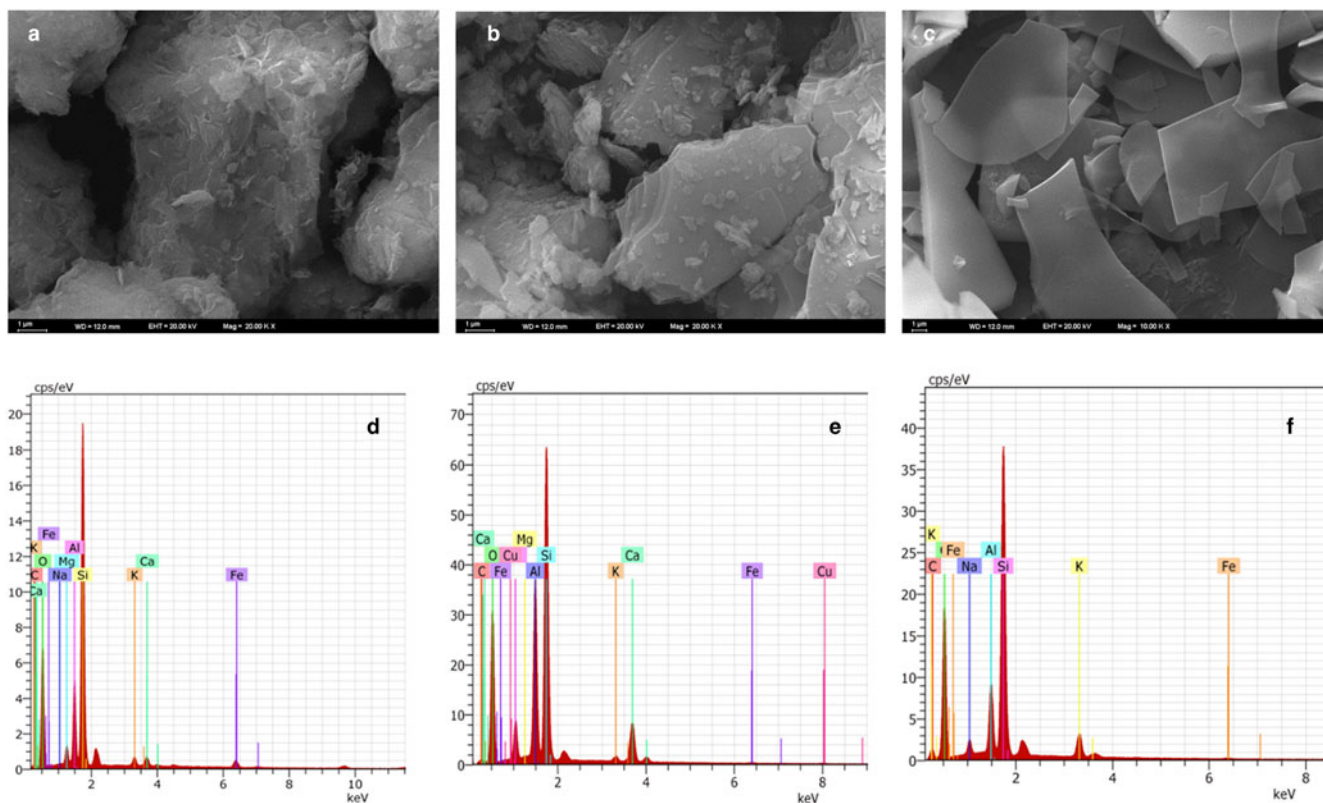


**Figure 4.** SEM images of (a) bentonite (20,000 $\times$  magnification), (b) zeolite (20,000 $\times$  magnification) and (c) perlite (10,000 $\times$  magnification) and EDS analyses of (d) bentonite, (e) zeolite and (f) perlite.

**Table 2.** Elemental composition (wt.%) of the adsorbent materials as obtained from EDS.

Adsorbent	Na	Mg	Al	Si	K	Ca	Fe	C	O
Bentonite	0.59	2.40	8.64	30.44	2.22	2.99	7.18	1.82	43.72
Zeolite	5.26	0.48	15.38	25.40	0.76	6.46	0.63	1.38	43.86
Perlite	7.99	–	11.28	39.70	5.34	–	0.49	0.16	35.05

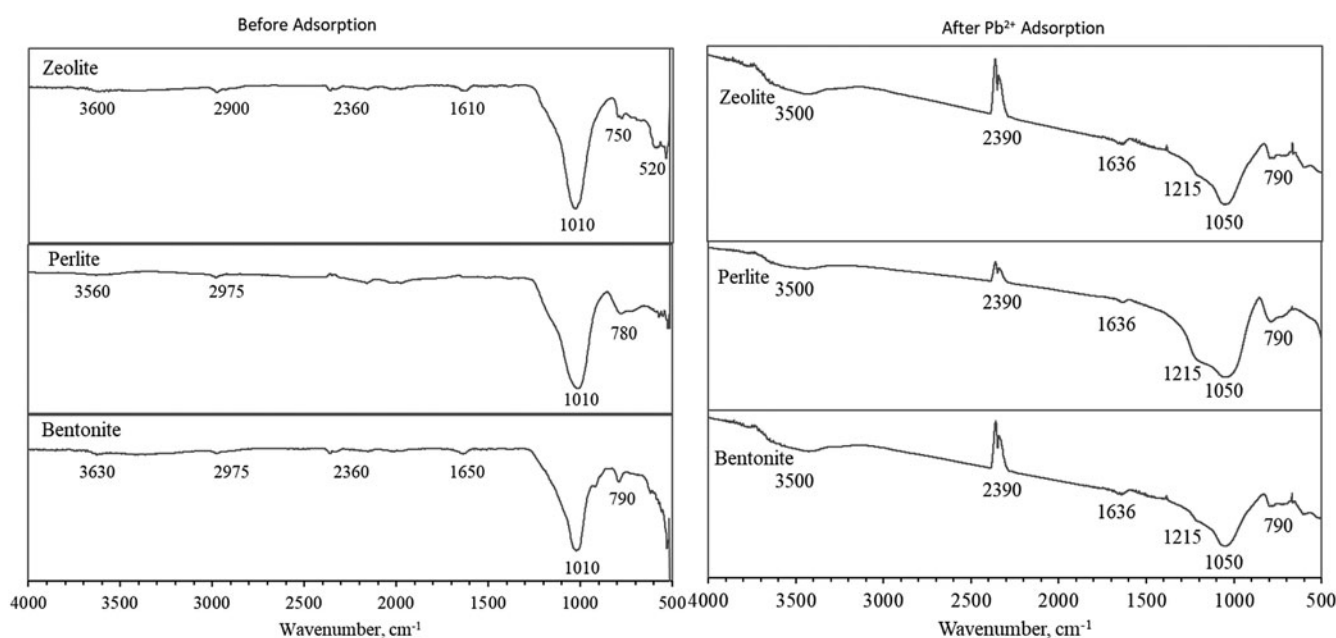
sizes in the ranges of 1.97–2.76 g cm<sup>-3</sup> and 21.6–34.7 μm, respectively. As is known, the water absorption capacity, CEC and BET surface area of the materials are the main physicochemical properties to consider when an adsorbent is being selected for the remediation of contaminated water sources. Although these properties affect the adsorption capacity, these data should be evaluated together with the adsorption capacity data attained from the batch adsorption experiments. If the BET surface area is high in addition to the water absorption capacity of the material being high, contaminated water is transferred more into the pores and the adsorbate has a greater chance of exchanging with the cations of the adsorbent materials. Bentonite (Fig. 4a), having the greatest BET surface area (85.25 m<sup>2</sup> g<sup>-1</sup>), had the highest CEC (40.63 meq 100 g<sup>-1</sup>). Perlite (Fig. 4c), on the other hand, having the greatest water absorption capacity (58.2%), had the lowest CEC (7.81 meq 100 g<sup>-1</sup>) and BET (3.42 m<sup>2</sup> g<sup>-1</sup>) values. CEC has been reported in the literature as 65 and 108 meq 100 g<sup>-1</sup> (Özgülven *et al.*, 2020), 74 meq 100 g<sup>-1</sup> (Tabak *et al.*, 2011), 85 meq 100 g<sup>-1</sup> (Rouliia & Vassiliadis, 2008) and 33.2 meq 100 g<sup>-1</sup> (Juang *et al.*, 2004) for bentonite, 2.7–3.2 mg g<sup>-1</sup> (Delkash *et al.*, 2015), 60.5 and 57.2 meq 100 g<sup>-1</sup> (Yukselen-Aksoy, 2010), 2.60–2.80 meq g<sup>-1</sup> (Krol, 2019) and 12 mmol 100 g<sup>-1</sup> (Andryushchenko *et al.*, 2017) for zeolite, 6 mmol 100 g<sup>-1</sup> (Andryushchenko *et al.*, 2017), 25 meq 100 g<sup>-1</sup> (Rouliia & Vassiliadis, 2008) and 25.9 meq 100 g<sup>-1</sup> (Alkan *et al.*, 2005) for perlite and 35 meq 100 g<sup>-1</sup> (Rouliia & Vassiliadis, 2008) and 33.3 meq 100 g<sup>-1</sup> (Alkan *et al.*, 2005) for expanded perlite. BET surface areas have been given as 27 and 43 m<sup>2</sup> g<sup>-1</sup>

**Table 3.** Physicochemical analyses of bentonite, zeolite and perlite.

Physicochemical property	Bentonite	Zeolite	Perlite
Density (g cm <sup>-3</sup> )	2.76	2.65	1.97
Mean particle size (μm)	21.6	34.7	32.1
CEC (meq 100 g <sup>-1</sup> )	40.63	9.36	7.81
Water absorption capacity (%)	58.2	23.8	71.1
Dissolution (%)	27.05	15.07	8.71
BET surface area (m <sup>2</sup> g <sup>-1</sup> )	85.25	17.06	3.42
PZC	4.50	5.03	5.21
ζ-potential (pH = 7)	-11.8	-23.4	-59.6

(Özgülven *et al.*, 2020), 43.1 m<sup>2</sup> g<sup>-1</sup> (Rouliia & Vassiliadis, 2008), 35.5 m<sup>2</sup> g<sup>-1</sup> (Anirudhan & Ramachandran, 2015), 29.5 m<sup>2</sup> g<sup>-1</sup> (Li *et al.*, 2009) and 226–318 m<sup>2</sup> g<sup>-1</sup> (Juang *et al.*, 2004) for bentonite, 35.85 m<sup>2</sup> g<sup>-1</sup> (Roshanfekr Rad & Anbia, 2021), 13.69 m<sup>2</sup> g<sup>-1</sup> (Wijesinghe *et al.*, 2016) and 140 m<sup>2</sup> g<sup>-1</sup> (Nurliati *et al.*, 2015) for natural zeolite, 1.30 m<sup>2</sup> g<sup>-1</sup> (Rouliia & Vassiliadis, 2008), 1.92 m<sup>2</sup> g<sup>-1</sup> (Irani *et al.*, 2011) and 1.22 m<sup>2</sup> g<sup>-1</sup> (Doğan *et al.*, 1997) for perlite and 4.70 m<sup>2</sup> g<sup>-1</sup> (Rouliia & Vassiliadis, 2008) and 2.30 m<sup>2</sup> g<sup>-1</sup> (Doğan *et al.*, 1997) for expanded perlite. As can be seen, the CEC and BET values varied significantly among these previous studies. This is due to the chemical structure and composition of the adsorbent varying with its origin.

PZC and ζ-potential are the other important parameters for adsorbents, as pH affects both the formation of lead compounds and the surface charge of the adsorbent. PZC was calculated to determine the pH value at which the positive and negative charges are equal and ζ-potential was calculated to determine the potential difference between the dispersion medium and the stationary layer of the fluid of the adsorbent, indicating the charge present on the adsorbent. At lower pH levels, H<sup>+</sup> ions were adsorbed more than the other cations (adsorbate), leading to a positively charged surface. In contrast, at greater pH levels, OH<sup>-</sup> ions increased, leading to a negatively charged surface. By determining the PZC and ζ-potential, the experimental pH was selected to be in line with the preferred surface charge. For instance, during the

**Figure 5.** FTIR spectra of the adsorbents before and after Pb<sup>2+</sup> ion adsorption.

**Table 4.** Elemental analysis results of the dissolved elements of the adsorbents (ppm).

Adsorbent	Na	Mg	Al	K	Ca	Fe
Bentonite	2.40	0.48	2.54	0.63	0.48	0.26
Perlite	2.21	0.08	0.01	0.61	0.60	0.07
Zeolite	1.41	0.16	1.01	0.48	0.76	0.14
Milli-Q	0.73	0.03	0.01	0.00	0.03	0.07

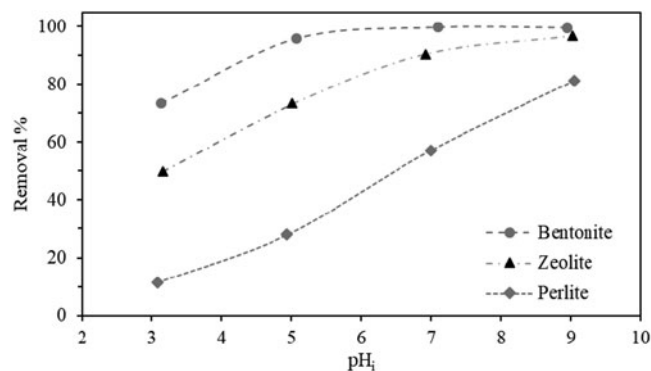
adsorption of the  $Pb^{2+}$  ions, a negatively charged surface is desired so that the adsorption capacity of the adsorbent increases, enabling adsorption of cations through electrostatic attraction in addition to cation exchange. As can be seen from Table 3, the PZC values of all of the adsorbents were less than pH 7, indicating that the surface charges of the adsorbents were negative above their respective PZC values. The  $\zeta$ -potentials being negative at pH 7 also supported this finding. The increase in the PZC values and the decrease in the  $\zeta$ -potential values (Table 3) were observed to become greater with the amount of the exchangeable cations ( $K^+$ ,  $Na^+$ ,  $Ca^{2+}$ ,  $Mg^{2+}$ ; Tables 1 & 2). The PZC values have been reported in the literature as 3.0 (Mekhamer, 2010) and 6.3 (Li *et al.*, 2009) for bentonite, 6.24–6.47 (Eberle *et al.*, 2022), 4.7 (Roshanfekar Rad & Anbia, 2021) and 2.2 (Nguyen *et al.*, 2015) for natural zeolite and 4.3 (Irani *et al.*, 2011) for perlite, all below pH 7. Besides these studies, reports have shown  $\zeta$ -potentials of  $<0$  within all of the studied pH ranges for bentonite (Onen & Gocer, 2019), zeolite (Yu *et al.*, 2013) and perlite (Doğan *et al.*, 1997).

While selecting the correct adsorbent for the remediation studies, the dissolution of the adsorbent should be controlled so as not to contaminate the water sources with the unwanted (toxic) ions released from the adsorbent materials. As can be seen in Table 3, bentonite demonstrated the greatest dissolution percentage, and so greatest amount of ions released into the environment (Table 4). As is shown, aluminium was released from bentonite (2.54 ppm) and zeolite (1.01 ppm), which could limit their use if they are to be used in large amounts. The results of the analysis of Milli-Q water before the dissolution test are also given in Table 4 for comparison.

### Batch adsorption experiments using stable $Pb^{2+}$ ions

#### Effect of initial pH of the solution on $Pb^{2+}$ ion adsorption

Initial pH is one of the most important parameters on  $Pb^{2+}$  ion adsorption, as pH affects both the formation of lead compounds

**Figure 6.** Effect of pH on the adsorption of  $Pb^{2+}$  ions using bentonite, zeolite and perlite. Adsorption conditions: initial concentration of  $Pb^{2+}$  = 200 ppm; adsorbent dosage = 5 g L<sup>-1</sup>; contact time = 1440 min; temperature = 25°C; shaking rate = 75 rpm.

and the surface charge of the adsorbent. The effect of the initial pH of the solution (pH<sub>i</sub>) on the adsorption of  $Pb^{2+}$  ions from the contaminated aqueous solution by bentonite, perlite and zeolite was investigated in the pH range of 3.0–9.0 at 25°C for 1440 min, an initial  $Pb^{2+}$  ion concentration of 200 ppm, a shaking rate of 75 rpm and an adsorbent dosage of 5 g L<sup>-1</sup>. As can be seen in Fig. 6, the removal percentage in terms of  $Pb^{2+}$  ion adsorption increased from 50% to 97% for zeolite and from 12% to 81% for perlite in the pH range of 3.0–9.0, whereas it increased from 74% to 96% in the pH range of 3.0–5.0 and further increased to 100% at pH 7.0–9.0 for bentonite. The low removal percentages at low pH values (pH < PZC) are due to the electrostatic repulsion between  $Pb^{2+}$  ions and the edge groups with a positive charge (Si–OH<sup>2+</sup>) on the surface of the adsorbents and to the excess amount of H<sub>3</sub>O<sup>+</sup> ions in the solution (Sharifipour *et al.*, 2015). The adsorption of  $Pb^{2+}$  at pH < 6 can be attributed to the ion exchange between  $Pb^{2+}$  and H<sup>+</sup>/M<sup>n+</sup> on the surface ion-exchange sites (Bourliva *et al.*, 2013). From the Pourbaix diagram of lead (Lehto & Hou, 2010), it can be seen that lead exists in the form of  $Pb^{2+}$  until pH 7.5 and as PbOH<sup>+</sup> in the pH range of 7.5–9.5. Hence, the initial pH of the solution was set at 7.0 in all of the batch adsorption experiments.

The  $\zeta$ -potentials of all adsorbents were found to be negative at pH 7.0 (Table 3), implying a negative potential difference between the dispersion medium and the stationary layer of the fluid of the adsorbent. Thus, the removal of lead can be caused by electrostatic attraction between the negatively charged adsorbent surface and the positively charged  $Pb^{2+}$  ions and also by ion exchange. In a study performed at pH 4–6 by Mao *et al.* (2023), it has been shown that  $Pb^{2+}$  was adsorbed by various minerals in the following order: montmorillonite > goethite > ferrihydrite > kaolinite. It was stated that due to its high electronegativity and typical CEC, montmorillonite had excellent adsorption properties (69.20 mg g<sup>-1</sup> at pH 6.0; Mao *et al.*, 2023), which was similar to that observed in the present study.

#### Effect of contact time on $Pb^{2+}$ ion adsorption

To investigate the effect of contact time on  $Pb^{2+}$  ion adsorption, the experiments were carried out at pH 7.0, temperature 25°C for 15–1440 min, an initial  $Pb^{2+}$  ion concentration of 400 ppm, a shaking rate of 75 rpm and an adsorbent dosage of 5.0 g L<sup>-1</sup>. As can be seen in Fig. 7, there was a rapid increase in the adsorption of lead on the adsorbents with increasing contact time, with the majority of the metal ions being adsorbed in the first 15 min. The removal percentage of  $Pb^{2+}$  ions increased from 92% (15 min) to 95% (120 min) for bentonite, from 40% (15 min) to 42% (60 min) for zeolite and from 19% (15 min) to 27% (60 min) for perlite. After the stated contact times, the removal percentages did not change as all of the available adsorbing sites on the adsorbent surface were occupied with the metal ions. This can be attributed to the instantaneous saturation of the adsorbent surface and the achievement of equilibrium within the first 1–2 h. Therefore, the contact time was set to 120 min in each experiment.

#### Effect of adsorbent dosage on $Pb^{2+}$ ion adsorption

The effects of the adsorbent dosage on the adsorption of  $Pb^{2+}$  ions by bentonite, zeolite and perlite are given in Fig. 8. The amount of adsorbent dosage was varied between 1 and 10 g L<sup>-1</sup> at pH 7.0, temperature 25°C, a contact time of 120 min, a shaking rate of 75 rpm and an initial  $Pb^{2+}$  ion concentration of 400 ppm. It is apparent that the removal percentage of  $Pb^{2+}$  ions increased with



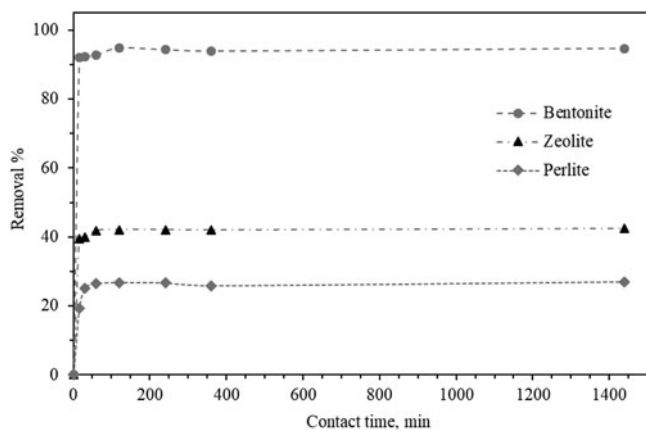


**Figure 7.** Effect of contact time on the adsorption of Pb<sup>2+</sup> ions using bentonite, zeolite and perlite. Adsorption conditions: initial concentration of Pb<sup>2+</sup> = 400 ppm; adsorbent dosage = 5 g L<sup>-1</sup>; temperature = 25°C; shaking rate = 75 rpm; pH = 7.

respectively. Although it is advantageous to achieve a progressive increase in the removal percentages with increasing adsorbent dosage, it should be noted that the ions that are released into the solution (Table 4) also increase with the adsorbent dosage, which may increase the contamination of the aqueous solution.

*Effect of initial Pb<sup>2+</sup> ion concentration on Pb<sup>2+</sup> ion adsorption: adsorption isotherms*

The effect of initial Pb<sup>2+</sup> ion concentration on Pb<sup>2+</sup> ion adsorption was studied by varying the initial Pb<sup>2+</sup> ion concentrations between 100 and 800 ppm at pH 7.0, temperature 25°C, a contact time of 120 min, a shaking rate of 75 rpm and an adsorbent dosage of 5 g L<sup>-1</sup>. As can be seen in Fig. 9, the adsorption capacity increased with increasing initial Pb<sup>2+</sup> ion concentration. This is due to the fact that the mass transfer driving force becomes greater at greater initial adsorbate concentrations (Fayazi *et al.*, 2019). At greater Pb<sup>2+</sup> ion concentrations, the number of Pb<sup>2+</sup> ions that will interact with the active sites on the surfaces of the

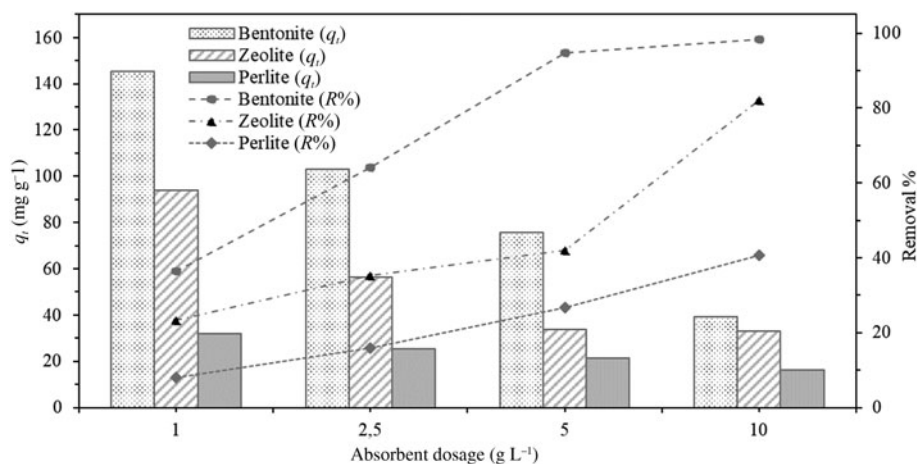


**Figure 8.** Effect of adsorbent dosage on the adsorption of Pb<sup>2+</sup> ions using bentonite, zeolite and perlite. Adsorption conditions: initial concentration of Pb<sup>2+</sup> = 400 ppm; temperature = 25°C; shaking rate = 75 rpm; pH = 7; contact time = 120 min.

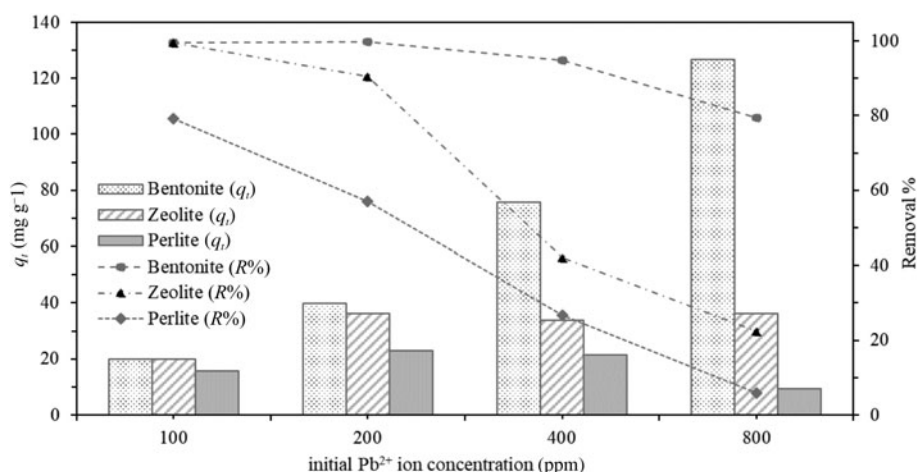


**Figure 9.** Effect of initial Pb<sup>2+</sup> ion concentration on the adsorption of Pb<sup>2+</sup> ions using bentonite, zeolite and perlite. Adsorption conditions: temperature = 25°C; shaking rate = 75 rpm; pH = 7; contact time = 120 min; adsorbent dosage = 5 g L<sup>-1</sup>.

increasing adsorbent dosage (i.e. increasing the number of unsaturated adsorption sites) and hence the metal ion concentration in the solution decreased. Bentonite, having the greatest BET surface area (Table 3), had a removal percentage of 95% at the adsorbent dosage of 5 g L<sup>-1</sup>. On the other hand, zeolite and perlite had removal percentages of 82% and 41% at the adsorbent dosage of 10 g L<sup>-1</sup>,

adsorbent materials increases, which, after some time, causes the adsorbent surface to reach saturation, leading to a decrease in the removal percentage. The removal percentages of adsorbents at 400 ppm initial Pb<sup>2+</sup> ion concentration were found to be 95%, 27% and 42% for bentonite, zeolite and perlite, respectively. These percentages dropped drastically at 800 ppm for zeolite and perlite;

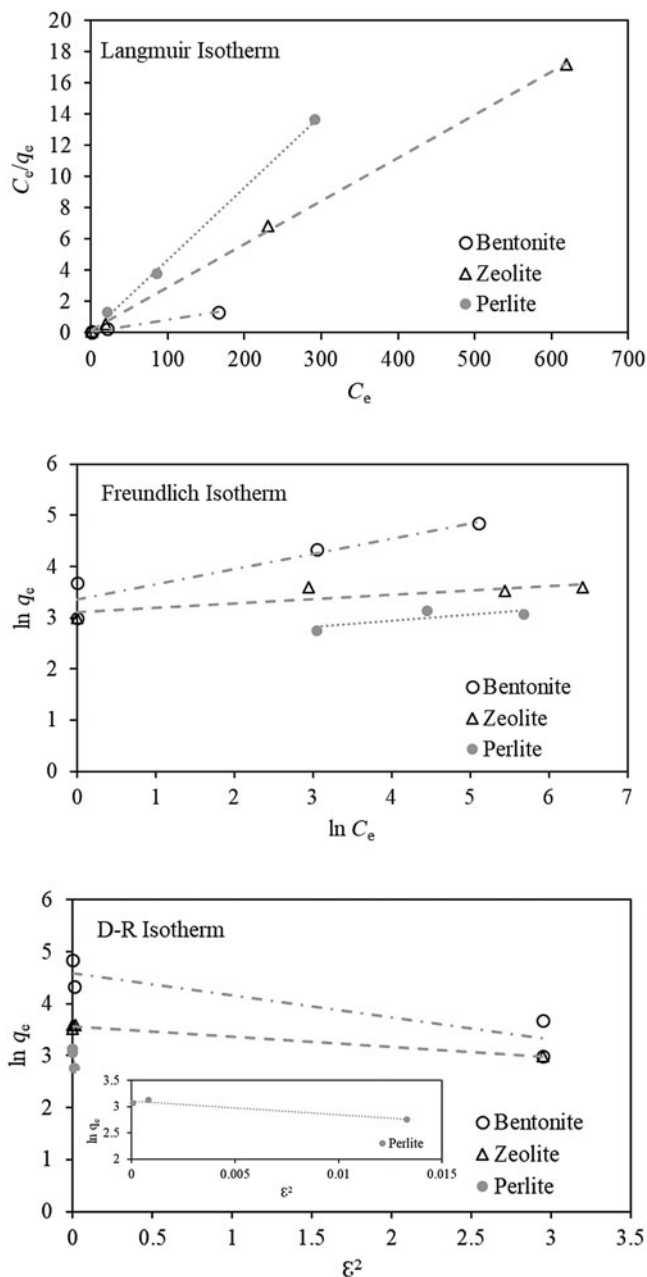


**Figure 10.** Isotherm models for  $Pb^{2+}$  adsorption on bentonite, zeolite and perlite. D-R = Dubinin–Radushkevich isotherm.

however, a removal percentage of 79% was reached for bentonite at this initial concentration.

The isotherm studies provide information on the adsorption capacities of the adsorbents, which is the most essential parameter in adsorption studies. The adsorption capacities obtained at varying ion concentrations for each adsorbent were used to evaluate certain constants that characterize the adsorption system. The experimental data regarding  $q_e$  and  $C_e$  were correlated using the linear forms of the Langmuir, Freundlich and Dubinin–Radushkevich isotherms (Fig. 10 & Table 5). By considering the correlation coefficients ( $R^2$ ), it was observed that the Langmuir isotherm showed the best correlation within the studied concentration range for all adsorbents. The maximum adsorption capacities were 131.6, 36.1 and 21.5  $mg\ g^{-1}$  for bentonite, zeolite and

perlite, respectively. Their fit to the Langmuir isotherm confirms that the adsorption of  $Pb^{2+}$  ions on the adsorbents occurred through a single layer establishing the chemical bonds. Previous studies on the adsorption of  $Pb^{2+}$  ions from aqueous solutions using bentonite, perlite and zeolite reported similar results in the literature. Some of the maximum adsorption capacities found in the literature are compared with the results from this study in Table 6.

#### Effect of temperature on $Pb^{2+}$ ion adsorption: adsorption thermodynamics

The effect of temperature on the adsorption of  $Pb^{2+}$  ion by bentonite, zeolite, and perlite was studied at temperatures of 25–60°C, pH 7.0 for 120 min, adsorbent dosage of 5 g/L, shaking rate of 75 rpm, and the initial  $Pb^{2+}$  ion concentration of 400 ppm. It was found that the removal percentage of bentonite and perlite changed slightly (0.9% for bentonite and 0.1% for perlite) with increasing temperature. However, the removal percentage of zeolite was increased from 42% (25°C) to 53% (60°C).

Thermodynamic parameters such as the Gibbs free energy change ( $\Delta G^\circ$ ), enthalpy change ( $\Delta H^\circ$ ) and entropy change ( $\Delta S^\circ$ ) of adsorption were evaluated using Equations 4–6 (Table 7), with  $\Delta H^\circ$  and  $\Delta S^\circ$  being obtained from the slope and intercept of the  $\ln K_d - 1/T$  plot (Fig. 11). The Gibbs free energy change ( $\Delta G^\circ$ ) indicates the degree of spontaneity of the adsorption process, enthalpy change ( $\Delta H^\circ$ ) shows whether the adsorption is exothermic or endothermic and entropy change ( $\Delta S^\circ$ ) reflects the degree of randomness. As can be seen in Table 7, adsorption occurred spontaneously for all of the adsorbents, with this behaviour increasing with increasing temperature. It was also observed that the process was endothermic and its randomness at the solid/liquid interface increased during the adsorption of  $Pb^{2+}$  ions onto the adsorbents.

#### Effect of shaking rate on $Pb^{2+}$ ion adsorption

The effect of shaking rate on  $Pb^{2+}$  ion adsorption was studied by varying the shaking rate between 0 and 150 rpm at pH 7.0, temperature 25°C, a contact time of 120 min, an adsorbent dosage of 5 g  $L^{-1}$  and a  $Pb^{2+}$  ion concentration of 400 ppm. As can be observed, the removal percentages increased from 67%, 39% and 8% (0 rpm) to 95%, 42% and 27% (75 rpm) for bentonite, zeolite and perlite, respectively (Fig. 12). In addition, increasing the shaking rate to 150 rpm did not affect the removal percentages for all adsorbents. Increasing the shaking rate also had a positive impact on  $Pb^{2+}$  ion adsorption, as has been reported previously in the literature (Murithi *et al.*, 2012; Shaheen *et al.*, 2016).

#### Characterization of the adsorbents after $Pb^{2+}$ ion adsorption

The adsorbents containing  $Pb^{2+}$  ions after the batch adsorption experiment at pH 7, a contact time of 120 min, an adsorbent dosage of 5 g  $L^{-1}$ , a shaking rate of 75 rpm and a temperature of 25°C using an initial  $Pb^{2+}$  ion concentration of 400 ppm were examined with XRF (Table 1) and FTIR (Fig. 5) analyses. The XRF analysis showed that  $Pb^{2+}$  was adsorbed onto the surfaces of bentonite (5.4%), zeolite (2.3%) and perlite (0.5%) successfully either by electrostatic interaction or by ion exchange. The decrease in the elemental percentages of Na, Mg, K and Ca indicated that these elements were exchanged with  $Pb^{2+}$  ions. The FTIR spectra of bentonite, zeolite and perlite also showed the exchange process between  $Pb^{2+}$  and the exchangeable cations through the changes

**Table 5.** Isotherm models, model constants and coefficients of correlation ( $R^2$ ) for the adsorption of  $Pb^{2+}$  ions onto bentonite, zeolite and perlite.

Isotherm model <sup>a</sup>	Model constants	Bentonite	Zeolite	Perlite	
Langmuir	Non-linear equation: $q_e = \frac{q_m K_L C_e}{1 + K_L C_e}$	$q_m$ (mg g <sup>-1</sup> )	131.6	36.1	21.5
	Linear equation: $\frac{C_e}{q_e} = \frac{1}{K_L q_m} + \frac{C_e}{q_m}$	$K_L$ (L mg <sup>-1</sup> )	0.13	0.23	0
		$R^2$	0.995	0.999	0.998
Freundlich	Non-linear equation: $q_e = K_F C_e^{1/n}$	$n$	3.3	11.8	8.2
	Linear equation: $\ln(q_e) = \ln(K_F) + \frac{\ln(C_e)}{n}$	$K_F$ ( $\frac{mg}{g} (\frac{L}{mg})^{1/n}$ )	28.48	22.30	11.56
		$R^2$	0.870	0.703	0.642
Dubinin–Radushkevich	Non-linear equation: $q_e = q_m e^{-K' \epsilon^2}$	$q_m$ (mmol g <sup>-1</sup> )	98.38	35.35	22.32
	Linear equation: $\ln(q_e) = \ln(q_m) - K' \epsilon^2$	$K'$ (mol <sup>2</sup> kJ <sup>-2</sup> )	0.43	0.20	26.31
		$E$ (kJ mol <sup>-1</sup> )	1.08	1.60	0.14
		$R^2$	0.807	0.986	0.956

<sup>a</sup>  $q_m$  is the maximum adsorption capacity of the adsorbents,  $K_L$  and  $K_F$  are the adsorption coefficients,  $n$  is the Freundlich constant,  $K'$  is the adsorption energy constant,  $E$  is the average adsorption energy ( $E = 1/(2K')^{1/2}$ ) and  $\epsilon$  is the adsorption potential (kJ mol<sup>-1</sup>;  $\epsilon = RT \ln(1 + 1/C_e)$ ).

**Table 6.** Pb(II) adsorption capacities of bentonite zeolite and perlite reported in the literature.

Adsorbent	Adsorption capacity (mg g <sup>-1</sup> )	Reference
Bentonite	131.6	This study
Bentonite	149.3	Hamadneh <i>et al.</i> (2015)
Raw bentonite	64.29	Eren <i>et al.</i> (2009)
Acid-activated bentonite	40.14	Eren <i>et al.</i> (2009)
Bentonite	68.8	Randelović <i>et al.</i> (2012)
Activated bentonite	6.5	Pawar <i>et al.</i> (2016)
Zeolite (clinoptilolite)	36.1	This study
Raw zeolite (clinoptilolite)	80.9	Günay <i>et al.</i> (2007)
Zeolite	78.6	Wang <i>et al.</i> (2008)
Zeolite	14.2	Rakhym <i>et al.</i> (2020)
Zeolite	25.3	Sharifpour <i>et al.</i> (2015)
Pretreated zeolite (clinoptilolite)	122.4	Günay <i>et al.</i> (2007)
Perlite (expanded)	21.5	This study
Expanded perlite	6.27	Ghassabzadeh <i>et al.</i> (2010)
Perlite	8.9	Irani <i>et al.</i> (2011)
Expanded perlite	13.4	Sari <i>et al.</i> (2007)

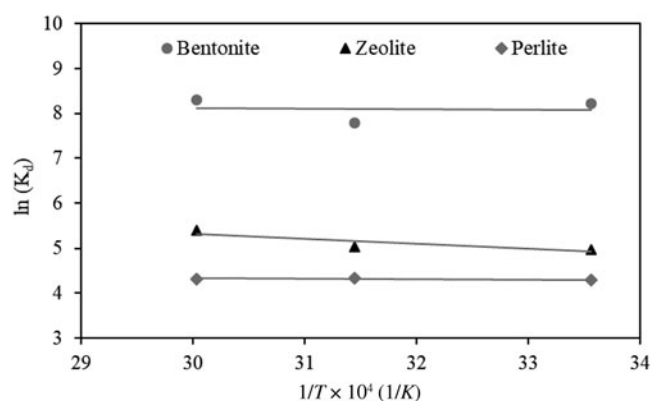
in the positions and shapes of the fundamental vibrations of the OH and Si–O groups. For instance, the stretching OH band at 3630–3560 cm<sup>-1</sup> shifted to 3500 cm<sup>-1</sup> for Pb<sup>2+</sup>-saturated samples, showing a broad band of water due to the overlapping of (H–O–H) stretching vibrations, and the absorption near 1636 cm<sup>-1</sup> (H–O–H) bending vibrations confirmed the presence of the Pb<sup>2+</sup> ions in the previously vacant sites. The band near 2360 cm<sup>-1</sup> also shifted to 2390 cm<sup>-1</sup>, giving a sharp peak for Pb<sup>2+</sup>-saturated samples. The band near 1010 cm<sup>-1</sup> assigned to Si–O stretching vibrations moved to 1050 cm<sup>-1</sup> after Pb<sup>2+</sup> ion adsorption, suggesting the interaction of the minerals with Pb<sup>2+</sup>. The involvement of Si–O–Si and OH present in the clay in interaction with Pb<sup>2+</sup> has also been reported previously (Hannachi *et al.*, 2013; Kushwaha *et al.*, 2019). The distinctions in the OH vibrational peaks are due to the differences in the binding abilities of Pb<sup>2+</sup> cations towards the interlayer water molecules, as they are preferably coordinated with the interlayer cations, and the residual water is retained by the interlayer holes. The water molecules coordinating with the cations can emigrate to the bi-trigonal cornered holes on the siloxane surface, affecting the OH groups and thus changing the intensities of the corresponding peaks (Tabak *et al.*, 2011).

**Table 7.** The thermodynamic parameters for Pb<sup>2+</sup> ion adsorption onto bentonite, zeolite and perlite.

Adsorbent	$\Delta H^\circ$ (kJ mol <sup>-1</sup> )	$\Delta S^\circ$ (J (mol·K) <sup>-1</sup> )	$\Delta G^\circ$ (kJ mol <sup>-1</sup> )		
			298 K	318 K	333 K
Bentonite	0.72	69.61	-20.35	-20.60	-22.99
Perlite	0.61	37.85	-10.65	-11.49	-11.96
Zeolite	9.37	72.41	-12.35	-13.30	-14.98

### Radioactive <sup>210</sup>Pb adsorption and determination of <sup>210</sup>Pb using the LSC system

The batch adsorption experiments were repeated with <sup>210</sup>Pb-contaminated (17.86 ± 1.28 Bq L<sup>-1</sup>) Pb<sup>2+</sup> ion solution having a concentration of 400 ppm at pH 7, a contact time of 120 min, an adsorbent dosage of 5 g L<sup>-1</sup>, a shaking rate of 75 rpm and a temperature of 25°C. <sup>210</sup>Pb, <sup>210</sup>Bi and <sup>210</sup>Po isotopes were present in radiochemical equilibrium in the stock solution of <sup>210</sup>Pb. Therefore, during the batch adsorption experiments, <sup>210</sup>Pb, <sup>210</sup>Bi and <sup>210</sup>Po isotopes were present in the solution, and <sup>210</sup>Bi and <sup>210</sup>Po could also be adsorbed on the surface of the adsorbents. The presence of <sup>210</sup>Pb and <sup>210</sup>Bi (β-emitters) and <sup>210</sup>Po (α-emitter) isotopes in the stock solution and the filtrates of the consecutive adsorption experiments using perlite can be seen in

**Figure 11.** The graph of  $\ln(K_d)$  as a function  $1/T$  for the adsorption of Pb<sup>2+</sup> ions using bentonite, zeolite and perlite. Adsorption conditions: shaking rate = 75 rpm; pH = 7; contact time = 120 min; adsorbent dosage = 5 g L<sup>-1</sup>; initial concentration of Pb<sup>2+</sup> = 400 ppm.

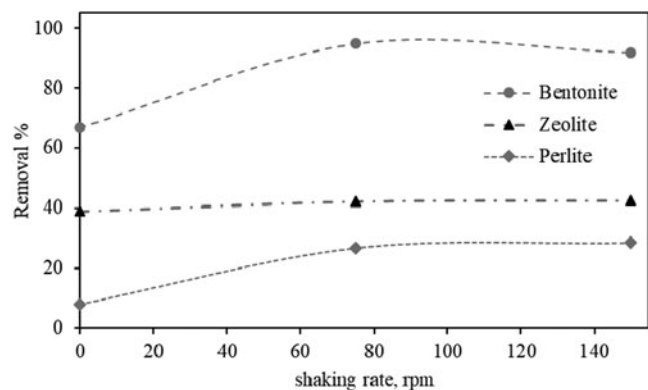


**Figure 12.** Effect of shaking rate on the adsorption of  $Pb^{2+}$  ions using bentonite, zeolite and perlite. Adsorption conditions: temperature = 25°C; pH = 7; contact time = 120 min; adsorbent dosage = 5 g L<sup>-1</sup>; initial concentration of  $Pb^{2+}$  = 400 ppm.

the  $\beta$ -spectra (Fig. 13a) and  $\alpha$ -spectra (Fig. 13b), respectively. The activity concentrations of  $^{210}Pb$  and  $^{210}Po$  isotopes, calculated by using Equation 7, are given in Table 8. As is known, the radiochemical equilibrium was disturbed after the first adsorption. Hence, the activity concentrations of  $^{210}Pb$ ,  $^{210}Bi$  and  $^{210}Po$  changed in the filtrate. Due to the short half-life of  $^{210}Bi$  (5.012 (5) days; Nucleide Lara, 2023) and the time interval between the adsorption and LSC measurements not being constant for all of

the adsorbents, the activity concentration of  $^{210}Bi$  was not reported.

As can be seen from Table 8, bentonite removed 95% of  $^{210}Pb$  and 75% of  $^{210}Po$  in the first adsorption experiment. The removal percentages after the second adsorption experiment were found to be >99% for both of the radionuclides, as the activity concentrations were below their corresponding MDC values. Additionally, the gross  $\beta$ -activity concentration of bentonite was also less than the  $MDC_{\beta}$  value, indicating that all  $\beta$ -emitters, including  $^{210}Bi$ , were also adsorbed on the surface of bentonite. The removal percentages of zeolite and perlite were lower than the removal percentage of bentonite in the first adsorption experiment. Zeolite adsorbed 38% of  $^{210}Pb$  and 60% of  $^{210}Po$ , whereas perlite adsorbed 30% of  $^{210}Pb$  and 74% of  $^{210}Po$ . However, the activity concentrations of  $^{210}Pb$  and  $^{210}Po$  were less than the  $MDC_{\beta}$  and  $MDC_{\alpha}$  values after the third and second adsorption experiments, respectively, demonstrating that >99% of the radionuclides were removed from the solution.

In this study, the removal percentages of the stable and radioactive  $Pb^{2+}$  ions under the same adsorption conditions were compared for all adsorbents. Even though the stable  $Pb^{2+}$  ion concentration was determined using ICP-OES and the radioactive  $^{210}Pb$  activity concentration was determined using LSC, the removal percentages were found to be within 5% of each other, as was expected, due to the fact that both of them are isotopes of the same element and they have the same chemical behaviour.

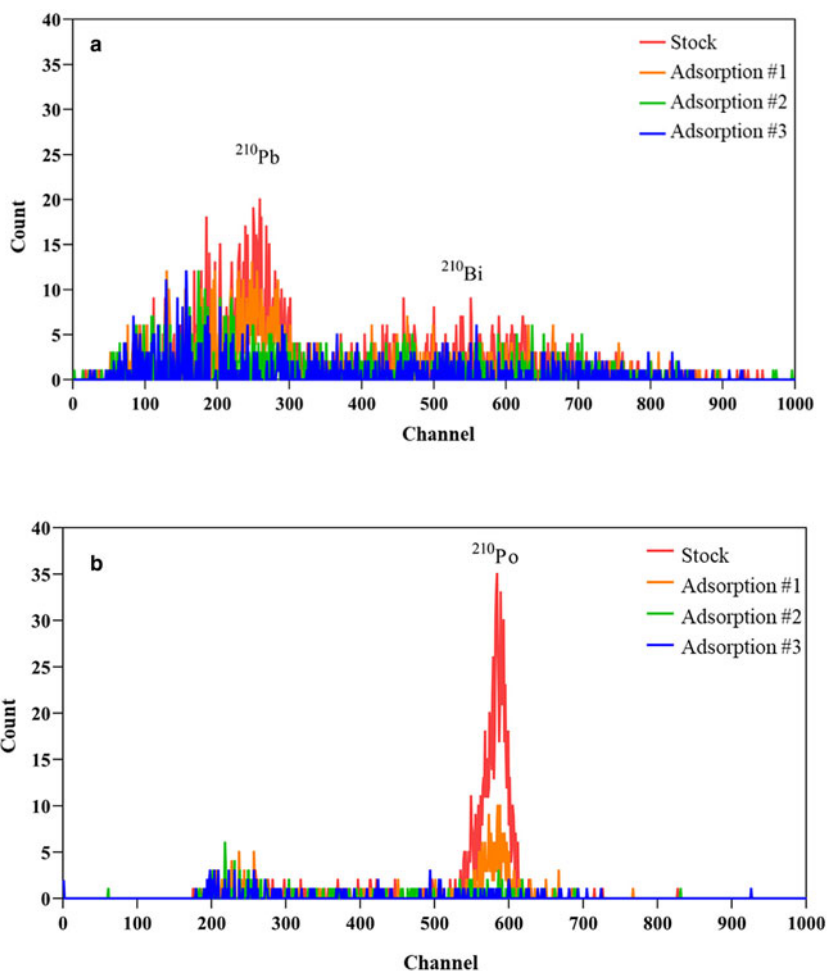


**Figure 13.** (a) Gross  $\beta$  and (b) gross  $\alpha$  LSC spectra of the stock solution and the filtrates of the successive batch adsorption experiments using perlite.



**Table 8.** The activity concentrations of  $^{210}\text{Pb}$  and  $^{210}\text{Po}$  in the stock solution and the filtrates of the successive batch adsorption experiments.

	Adsorption no.	$^{210}\text{Pb}$		$^{210}\text{Po}$	
		Activity concentration ( $\text{Bq L}^{-1}$ )	Removal (%)	Activity concentration ( $\text{Bq L}^{-1}$ )	Removal (%)
$^{210}\text{Pb}$ stock solution	–	$17.86 \pm 1.28$	–	$14.73 \pm 0.72$	–
Bentonite	1	$0.88 \pm 0.59$	95.07	$3.74 \pm 0.35$	74.61
	2	<MDC $_{\beta}$	>98.54	<MDC $_{\alpha}$	>99.79
Zeolite	1	$11.16 \pm 1.27$	37.51	$5.93 \pm 0.43$	59.74
	2	$3.17 \pm 1.09$	82.25	<MDC $_{\alpha}$	>99.79
	3	<MDC $_{\beta}$	>98.54	–	–
Perlite	1	$12.76 \pm 1.41$	29.56	$3.82 \pm 0.35$	74.07
	2	$2.02 \pm 1.10$	88.69	<MDC $_{\alpha}$	>99.79
	3	<MDC $_{\beta}$	>98.54	–	–

MDC $_{\alpha}$  = 0.03  $\text{Bq L}^{-1}$ ; MDC $_{\beta}$  = 0.26  $\text{Bq L}^{-1}$ .

## Conclusion

In this study, the  $\text{Pb}^{2+}$  adsorption capacities of bentonite, zeolite and perlite obtained from various locations in Türkiye were investigated. The results illustrated that the minerals had an adsorption capacity for  $\text{Pb}^{2+}$  in the following order: bentonite > zeolite > perlite. It was found that all minerals fit the Langmuir isotherm, indicating chemical bond formation between the adsorbent and  $\text{Pb}^{2+}$  ions during the adsorption process. The maximum adsorption capacities ( $q_m$ ) were found to be 131.6, 36.1 and 21.5  $\text{mg g}^{-1}$  for bentonite, zeolite and perlite, respectively. It should be mentioned that the adsorption of  $\text{Pb}^{2+}$  was a result of the ion exchange of the cations as observed from the FTIR analysis as well as the electrostatic attraction of  $\text{Pb}^{2+}$  ions to the adsorbent surface due to the negative surface charge of the adsorbents. It was also observed that the  $\text{Pb}^{2+}$  adsorption process was a spontaneous ( $\Delta G^\circ < 0$ ) and endothermic ( $\Delta H^\circ > 0$ ) process. Furthermore, the removal percentages of stable  $\text{Pb}^{2+}$  ions and radioactive  $^{210}\text{Pb}^{2+}$  isotopes by these minerals were compared using various analysis techniques. LSC ( $\beta$ -spectrometer) was used in an adsorption study for the first time. The removal percentages of radioactive  $^{210}\text{Pb}$  isotope were found to be 95%, 38% and 30% for bentonite, zeolite and perlite, respectively, which were in accordance with the stable  $\text{Pb}^{2+}$  ion removal percentage results of 95%, 42% and 27%. The LSC results showed that  $^{210}\text{Po}$  and  $^{210}\text{Bi}$  were also adsorbed on the surface of the minerals, with the removal percentages of  $^{210}\text{Po}$  being 75%, 60% and 74% for bentonite, zeolite and perlite, respectively. This study also showed the applicability of bentonite, zeolite and perlite to  $^{210}\text{Po}$  and  $^{210}\text{Bi}$  adsorption, which had not been demonstrated previously in the literature.

**Acknowledgements.** We thank MCL Bentonite for the bentonite samples, Prof Dr Yusuf Kağan Kadioğlu for the zeolite samples and Eti Mine Menderes Works for the expanded perlite samples, the Earth Sciences Application and Research Center (YEBİM) at Ankara University for the XRD, XRF and ICP-OES analysis support, Prof Dr Hande Çelebi at Eskişehir Technical University for the FTIR analysis support, the Institute of Nuclear Sciences at Ankara University for the SEM-EDS analysis support, Middle East Technical University (METU) Central Laboratory for the  $\zeta$ -potential and BET analysis support and the Superconductor Technologies Application and Research Center at Ankara University for the particle-size analysis support.

**Financial support.** This work was partially supported by Ankara University via project number BAP-21L0405003.

**Conflicts of interest.** The authors have no relevant financial or non-financial interests to disclose.

**Availability of data and materials.** Data are available upon request.

**Author contributions.** Conceptualization: G.Ö. Çakal; methodology: R. Güven, G.Ö. Çakal; formal analysis and investigation: O. Uygun, R. Güven, G.Ö. Çakal; supervision: G.Ö. Çakal; writing – original draft preparation: O. Uygun; writing – review and editing: R. Güven, G.Ö. Çakal.

## References

- Abdallah W. & Yilmazer U. (2011) Novel thermally stable organo-montmorillonites from phosphonium and imidazolium surfactants. *Thermochimica Acta*, **525**, 129–140.
- Abdullahi S.L. & Audu A.A. (2017) Comparative analysis on chemical composition of bentonite clays obtained from Ashaka and Tango deposits in Gombe State, Nigeria. *ChemSearch Journal*, **8**, 35–40.
- Aghabeyk F., Azadmehr A. & Hezarkhani A. (2022) Fabrication of feldspar-based geopolymers from perlite toward decontamination of heavy metals from aqueous solution: hydrolysis process, characterizations, kinetic and isotherm studies. *Journal of Environmental Chemical Engineering*, **10**, 108087.
- Albayati T.M., Sabri A.A. & Abed D.B. (2019) Adsorption of binary and multi heavy metals ions from aqueous solution by amine functionalized SBA-15 mesoporous adsorbent in a batch system. *Desalination and Water Treatment*, **151**, 315–321.
- Alkan M. & Doğan M. (2001) Adsorption of copper(II) onto perlite. *Journal of Colloid and Interface Science*, **243**, 280–291.
- Alkan M., Demirbaş Ö. & Doğan M. (2005) Zeta potential of unexpanded and expanded perlite samples in various electrolyte media. *Microporous and Mesoporous Materials*, **84**, 192–200.
- Anbia M., Kargosha K. & Khoshbooei S. (2015) Heavy metal ions removal from aqueous media by modified magnetic mesoporous silica MCM-48. *Chemical Engineering Research and Design*, **93**, 779–788.
- Andryushchenko N.D., Safonov A.V., Babich T.L., Ivanov P.V., Konevnik Y.V., Kondrashova A.A. *et al.* (2017) Sorption characteristics of materials of the filtration barrier in upper aquifers contaminated with radionuclides. *Radiochemistry*, **59**, 414–424.
- Anirudhan, T. & Ramachandran M. (2015) Adsorptive removal of basic dyes from aqueous solutions by surfactant modified bentonite clay (organoclay): kinetic and competitive adsorption isotherm. *Process Safety and Environmental Protection*, **95**, 215–225.
- Anokhina A., Aoki S., Ariga A., Arrabito L., Autiero D., Badertscher A. *et al.* (2008) Study of the effects induced by lead on the emulsion films of the OPERA experiment. *Journal of Instrumentation*, **3**, 1–17.
- ASTM 4646-03 (2016) *Standard Test Method for 24-h Batch-Type Measurement of Contaminant Sorption by Soils and Sediments*. ASTM International, West Conshohocken, PA, USA, 5 pp.
- ASTM C127-88 (1993) *Standard Test Method for Relative Density (Specific Gravity) and Absorption of Coarse Aggregate*. ASTM International, West Conshohocken, PA, USA, 6 pp.
- ASTM C837-09 (2009) *Standard Test Method for Methylene Blue Index of Clay*. ASTM International, West Conshohocken, PA, USA, 3 pp.

- Bakatula E.N., Richard D., Neculita C.M. & Zagury G.J. (2018) Determination of point of zero charge of natural organic materials. *Environmental Science and Pollution Research*, **25**, 7823–7833.
- Benhamou A., Baudu M., Derriche Z. & Basly J. (2009) Aqueous heavy metals removal on amine-functionalized Si-MCM-41 and Si-MCM-48. *Journal of Hazardous Materials*, **171**, 1001–1008.
- Bhattacharyya K.G. & Gupta S.S. (2008) Adsorption of a few heavy metals on natural and modified kaolinite and montmorillonite: a review. *Advances in Colloid and Interface Science*, **140**, 114–131.
- Bourliva A., Michailidis K., Sikalidis C., Filippidis A. & Betsiou M. (2013) Lead removal from aqueous solutions by natural Greek bentonites. *Clay Minerals*, **48**, 771–787.
- Çakal G.Ö., Güven R. & Yücel H. (2015) An application of LSC method for the measurement of gross alpha and beta activities in spiked water and drinking water samples. *Nukleonika*, **60**, 637–642.
- Çelik A.G., Kılıç A.M. & Çakal G.Ö. (2013) Expanded perlite aggregate characterization for use as a lightweight construction raw material. *Physicochemical Problems of Mineral Processing*, **49**, 689–700.
- Costafreda J.L. & Martín D.A. (2021) Bentonites in southern Spain. Characterization and applications. *Crystals*, **11**, 706.
- Delkash M., Ebrazi Bakhshayesh B. & Kazemian H. (2015) Using zeolitic adsorbents to cleanup special wastewater streams: a review. *Microporous and Mesoporous Materials*, **214**, 224–241.
- Detteri M., Arghittu A., Deiana G., Castiglia P. & Azara A. (2022) The revised European Directive 2020/2184 on the quality of water intended for human consumption. A step forward in risk assessment, consumer safety and informative communication. *Environmental Research*, **209**, 112773.
- Doğan M., Alkan M. & Çakir Ü. (1997) Electrokinetic properties of perlite. *Journal of Colloid and Interface Science*, **192**, 114–118.
- Donat R., Akdoğan A., Erdem E. & Cetisli H. (2005) Thermodynamics of Pb<sup>2+</sup> and Ni<sup>2+</sup> adsorption onto natural bentonite from aqueous solutions. *Journal of Colloid and Interface Science*, **286**, 43–52.
- Eberle S., Börnick H. & Stolte S. (2022) Granular natural zeolites: cost-effective adsorbents for the removal of ammonium from drinking water. *Water*, **14**, 939.
- El-Arish N., Zaki R.M., Miskan S., Setiabudi H. & Jaafar N. (2022) Adsorption of Pb(II) from aqueous solution using alkaline-treated natural zeolite: process optimization analysis. *Total Environment Research Themes*, **3–4**, 100015.
- Erdoğan Ş., Başaran Kankılıç G., Seyfe M., Tavşanoğlu Ü.N. & Akın Ş. (2023) Assessment of heavy metal pollution with different indices in Süreyyabey dam lake in Turkey. *Chemistry and Ecology*, **39**, 153–172.
- Eren E., Afsin B. & Onal Y. (2009) Removal of lead ions by acid activated and manganese oxide-coated bentonite. *Journal of Hazardous Materials*, **161**, 677–685.
- Ergin M., Saydam C., Basturk O., Erdem E. & Yoruk R. (1991) Heavy metal concentrations in surface sediments from the two coastal inlets (Golden Horn Estuary and Izmit Bay) of the northeastern Sea of Marmara. *Chemical Geology*, **91**, 269–285.
- EU (2020) Directive (EU) 2020/2184 Quality of water intended for human consumption (recast). Retrieved from <https://www.legislation.gov.uk/eudr/2020/2184>
- Fayazi M., Afzali D., Ghanei-Motlagh R. & Irajy A. (2019) Synthesis of novel sepiolite–iron oxide–manganese dioxide nanocomposite and application for lead(II) removal from aqueous solutions. *Environmental Science and Pollution Research*, **26**, 18893–18903.
- Fei Y. & Hu Y.H. (2023) Recent progress in removal of heavy metals from wastewater: a comprehensive review. *Chemosphere*, **335**, 139077.
- Fu F. & Wang Q. (2011) Removal of heavy metal ions from wastewaters: a review. *Journal of Environmental Management*, **92**, 407–418.
- Ghassabzadeh H., Torab-Mostaedi M., Mohaddespour A., Maragheh M.G., Ahmadi S.J. & Zaheri P. (2010) Characterizations of Co(II) and Pb(II) removal process from aqueous solutions using expanded perlite. *Desalination*, **261**, 73–79.
- Guerra D.J.L., Mello L., Resende R. & Silva R. (2013) Application as adsorbents of natural and functionalized Brazilian bentonite in Pb<sup>2+</sup> adsorption: equilibrium, kinetic, pH, and thermodynamic effects. *Water Resources and Industry*, **4**, 32–50.
- Günay A., Arslankaya E. & Tosun I. (2007) Lead removal from aqueous solution by natural and pretreated clinoptilolite: adsorption equilibrium and kinetics. *Journal of Hazardous Materials*, **146**, 362–371.
- Guo Y., Liu D., Zhao Y., Gong B., Guo Y. & Huang W. (2017) Synthesis of chitosan-functionalized MCM-41-A and its performance in Pb(II) removal from synthetic water. *Journal of the Taiwan Institute of Chemical Engineers*, **71**, 537–545.
- Hamadneh I., Abu-Zurayk R., Abu-Irmaileh B., Bozeya A. & Al-Dujaili A. (2015) Adsorption of Pb(II) on raw and organically modified Jordanian bentonite. *Clay Minerals*, **50**, 485–496.
- Hannachi Y., Homri T. & Boubaker T. (2013) Utilization of Tunisian bentonite as ion-exchange and sorbent material in the removal of lead from aqueous solutions. *The Holistic Approach to Environment*, **3**, 123–140.
- Hernández-Morales V., Nava R., Acosta-Silva Y., Macías-Sánchez S., Pérez-Bueno J. & Pawelec B. (2012) Adsorption of lead (II) on SBA-15 mesoporous molecular sieve functionalized with –NH<sub>2</sub> groups. *Microporous and Mesoporous Materials*, **160**, 133–142.
- Irani M., Amjadi M. & Mousavian M.A. (2011) Comparative study of lead sorption onto natural perlite, dolomite and diatomite. *Chemical Engineering Journal*, **178**, 317–323.
- Islam M.S., Ahmed M.K., Raknuzzaman M., Habibullah-Al-Mamun M. & Islam, M.K. (2015) Heavy metal pollution in surface water and sediment: a preliminary assessment of an urban river in a developing country. *Ecological Indicators*, **48**, 282–291.
- Jaishankar M., Tseten T., Anbalagan N., Mathew B.B. & Beeregowda K.N. (2014) Toxicity, mechanism and health effects of some heavy metals. *Interdisciplinary Toxicology*, **7**, 60–72.
- Joseph L., Jun B., Flora J.R., Park C.M. & Yoon Y. (2019) Removal of heavy metals from water sources in the developing world using low-cost materials: a review. *Chemosphere*, **229**, 142–159.
- Juang R., Lin S., Huang F. & Cheng, C. (2004) Structural studies of Na-montmorillonite exchanged with Fe<sup>2+</sup>, Cr<sup>3+</sup>, and Ti<sup>4+</sup> by N<sub>2</sub> adsorption and EXAFS. *Journal of Colloid and Interface Science*, **274**, 337–340.
- Khaleque A., Alam M.M., Hoque M., Mondal S., Haider J.B., Xu B. et al. (2020) Zeolite synthesis from low-cost materials and environmental applications: a review. *Environmental Advances*, **2**, 100019.
- Klopprogge J.T. (2017) Raman spectroscopy of clay minerals. Pp. 150–199 in: *Developments in Clay Science* (W.P. Gates, J.T. Klopprogge, J. Madejova & F. Bergaya, editors). Elsevier, Oxford, UK.
- Korkuna O., Lebeda R., Skubiszewska-Zieba J., Vrublevs'ka T., Gun'ko V. & Ryzkowski J. (2006) Structural and physicochemical properties of natural zeolites: clinoptilolite and mordenite. *Microporous and Mesoporous Materials*, **87**, 243–254.
- Krol M. (2019). Hydrothermal synthesis of zeolite aggregate with potential use as a sorbent of heavy metal cations. *Journal of Molecular Structure*, **1183**, 353–359.
- Kumar V., Dwivedi S. & Oh S. (2022) A critical review on lead removal from industrial wastewater: recent advances and future outlook. *Journal of Water Process Engineering*, **45**, 102518.
- Kushwaha A., Rani R. & Patra J.K. (2019) Adsorption kinetics and molecular interactions of lead [Pb(II)] with natural clay and humic acid. *International Journal of Environmental Science and Technology*, **17**, 1325–1336.
- Lehto J. & Hou X., editors (2010) *Chemistry and Analysis of Radionuclides: Laboratory Techniques and Methodology*. Wiley-VCH Verlag GmbH & Co. KGaA, Weinheim, Germany, 406 pp.
- Li J., Hu J., Sheng G., Zhao G. & Huang Q. (2009). Effect of pH, ionic strength, foreign ions and temperature on the adsorption of Cu(II) from aqueous solution to GMZ bentonite. *Colloids and Surfaces A: Physicochemical and Engineering Aspects*, **349**, 195–201.
- Limon S. (2016) *Determination of 210Pb and 210Po Activity Concentrations in Sediments by Using Radiochemical Separation Techniques*. MSc thesis, Ankara University, Türkiye.
- Lingamdinne L.P., Amelirad O., Koduru J.R., Karri R.R., Chang Y., Dehghani M.H. & Mubarak N.M. (2023) Functionalized bentonite for removal of Pb (II) and As(V) from surface water: predicting capability and mechanism using artificial neural network. *Journal of Water Process Engineering*, **51**, 103386.

- Liu C., Xu J., Liu C., Zhang P. & Dai M. (2009) Heavy metals in the surface sediments in Lanzhou reach of Yellow River, China. *Bulletin of Environmental Contamination and Toxicology*, **82**, 26–30.
- Mao X., Liu H., Chu Z., Chen T., Zou X., Chen D. *et al.* (2023) Adsorption of lead by kaolinite, montmorillonite, goethite and ferrihydrite: performance and mechanisms based on quantitative analysis. *Clay Minerals*, **57**, 230–240.
- Mekhamer W. (2010). The colloidal stability of raw bentonite deformed mechanically by ultrasound. *Journal of Saudi Chemical Society*, **14**, 301–306.
- Moshoeshe M., Nadiye-Tabbiruka M.S. & Obuseng V. (2017) A review of the chemistry, structure, properties and applications of zeolites. *American Journal of Materials Science*, **7**, 196–221.
- Murithi G., Onindo C.O. & Muthakia G.K. (2012) Kinetic and equilibrium study for the sorption of Pb(II) ions from aqueous phase by water hyacinth (*Eichhornia crassipes*). *Bulletin of the Chemical Society of Ethiopia*, **26**, 181–193.
- Nguyen T.C., Loganathan P., Nguyen T.V., Vigneswaran S., Kandasamy J. & Naidu R. (2015) Simultaneous adsorption of Cd, Cr, Cu, Pb, and Zn by an iron-coated Australian zeolite in batch and fixed-bed column studies. *Chemical Engineering Journal*, **270**, 393–404.
- Njoroge G.K., Njagi E.N.M., Orinda G.O., Sekadde-Kigundu C.B. & Kayima J.K. (2008) Environmental and occupational exposure to lead. *East African Medical Journal*, **85**, 284–291.
- Novikau R. & Lujanienė G. (2022) Adsorption behaviour of pollutants: heavy metals, radionuclides, organic pollutants, on clays and their minerals (raw, modified and treated): a review. *Journal of Environmental Management*, **309**, 114685.
- Nucleide Lara (2023) Library for gamma and alpha emissions. Retrieved from <http://www.nucleide.org/Laraweb/index.php>
- Nurliati G., Krisnandi Y.K., Sihombing R. & Salimin Z. (2015) Studies of modification of zeolite by tandem acid–base treatments and its adsorptions performance towards thorium. *Atom Indonesia*, **41**, 87–95.
- Onen V. & Gocer M. (2019) The effect of single and combined coagulation/flocculation methods on the sedimentation behavior and conductivity of bentonite suspensions with different swelling potentials. *Particulate Science and Technology*, **37**, 827–834.
- Özgüven F.E., Pekdemir A.D., Önal M. & Sarıkaya Y. (2020) Characterization of a bentonite and its permanent aqueous suspension. *Journal of the Turkish Chemical Society Section A: Chemistry*, **7**, 11–18.
- Pawar R.R., Lalhmunsiam Bajaj H.C. & Lee S.M. (2016) Activated bentonite as a low-cost adsorbent for the removal of Cu(II) and Pb(II) from aqueous solutions: batch and column studies. *Journal of Industrial and Engineering Chemistry*, **34**, 213–223.
- Pekey H. (2006) Heavy metal pollution assessment in sediments of the Izmit Bay, Turkey. *Environmental Monitoring and Assessment*, **123**, 219–231.
- Pereira E., Baptista-Neto J.A., Smith B.J. & McAllister J.J. (2007) The contribution of heavy metal pollution derived from highway runoff to Guanabara Bay sediments – Rio de Janeiro/Brazil. *Annals of the Brazilian Academy of Sciences*, **79**, 739–750.
- Raj K. & Das A.P. (2023) Lead pollution: impact on environment and human health and approach for a sustainable solution. *Environmental Chemistry and Ecotoxicology*, **5**, 79–85.
- Rakhym A., Seilkhanova G. & Kurmanbayeva T. (2020) Adsorption of lead (II) ions from water solutions with natural zeolite and chamotte clay. *Materials Today: Proceedings*, **31**, 482–485.
- Randelović M., Purenović M., Zarubica A., Purenović J., Matović B. & Momčilović M. (2012) Synthesis of composite by application of mixed Fe, Mg (hydr)oxides coatings onto bentonite – a use for the removal of Pb(II) from water. *Journal of Hazardous Materials*, **199–200**, 367–374.
- Roshanfekar Rad L. & Anbia M. (2021) Zeolite-based composites for the adsorption of toxic matters from water: a review. *Journal of Environmental Chemical Engineering*, **9**, 106088.
- Rouliam M. & Vassiliadis A.A. (2008) Sorption characterization of a cationic dye retained by clays and perlite. *Microporous and Mesoporous Materials*, **116**, 732–740.
- Sari A., Tuzen M., Citak D. & Soylak M. (2007) Adsorption characteristics of Cu(II) and Pb(II) onto expanded perlite from aqueous solution. *Journal of Hazardous Materials*, **148**, 387–394.
- Shaheen M.A., Akram R., Karim A., Mehmood T., Farooq R. & Iqbal M. (2016) Sequestering potential of peach nut shells as an efficient sorbent for sequestering some toxic metal ions from aqueous waste: a kinetic and thermodynamic study. *Pakistan Journal of Analytical & Environmental Chemistry*, **17**, 77–86.
- Sharifipour F., Hojati S., Landi A. & Cano A. (2015) Kinetics and thermodynamics of lead adsorption from aqueous solutions onto Iranian sepiolite and zeolite. *International Journal of Environmental Research*, **9**, 1001–1010.
- Tabak A., Yilmaz N., Eren E., Caglar B., Afsin B. & Sarihan A. (2011) Structural analysis of naproxen-intercalated bentonite (Unye). *Chemical Engineering Journal*, **174**, 281–288.
- Topal T. (1996) The use of methylene blue adsorption test to assess the clay content of the Cappadocian tuff. Presented at: *8th International Congress on the Deterioration and Conservation of Stone*, Berlin, Germany, 30 September–4 October.
- Unuabonah E., Adebowale K. & Olu-Owolabi B. (2007) Kinetic and thermodynamic studies of the adsorption of lead (II) ions onto phosphate-modified kaolinite clay. *Journal of Hazardous Materials*, **144**, 386–395.
- Velarde L., Nabavi M.S., Escalera E., Antti M. & Akhtar F. (2023) Adsorption of heavy metals on natural zeolites: a review. *Chemosphere*, **328**, 138508.
- Vicentin B.M. & Costa da Rocha R.D. (2021) Expanded perlite: potential for removing antibiotics from water. *Water SA*, **47**, 417–422.
- Vural A. (2015) Contamination assessment of heavy metals associated with an alteration area: Demirören Gumushane, NE Turkey. *Journal Geological Society of India*, **86**, 215–222.
- Wang S., Terdkiatburana T. & Tade M.O. (2008) Adsorption of Cu(II), Pb(II) and humic acid on natural zeolite tuff in single and binary systems. *Separation and Purification Technology*, **62**, 64–70.
- Wang S., Dong Y., He M., Chen L. & Yu X. (2009) Characterization of GMZ bentonite and its application in the adsorption of Pb(II) from aqueous solutions. *Applied Clay Science*, **43**, 164–171.
- WHO (2017) *Guidelines for Drinking-Water Quality*, 4th edition incorporating the first addendum. WHO Press, Geneva, Switzerland, 631 pp.
- Wijesinghe D.T.N., Dassanayake K.B., Sommer S.G., Jayasinghe G.Y., Scales P.J. & Chen D. (2016) Ammonium removal from high-strength aqueous solutions by Australian zeolite. *Journal of Environmental Science and Health, Part A*, **51**, 614–625.
- Yu Y., Murthy B.N., Shapter J.G., Constantopoulos K.T., Voelcker N.H. & Ellis A.V. (2013) Benzene carboxylic acid derivatized graphene oxide nanosheets on natural zeolites as effective adsorbents for cationic dye removal. *Journal of Hazardous Materials*, **260**, 330–338.
- Yukselen-Aksoy Y. (2010) Characterization of two natural zeolites for geotechnical and geoenvironmental applications. *Applied Clay Science*, **50**, 130–136.